Generation of sensory hair cells by genetic programming with a combination of transcription factors

Aida Costa[1,4], Luis Sanchez-Guardado[1,2], Stephanie Juniat[3], Jonathan Gale[3], Nicolas Daudet[3] and Domingos Henrique[1,2,*]

[1] *Instituto de Medicina Molecular, Faculdade de Medicina da Universidade de Lisboa, Portugal,*

[2] *Champalimaud Neuroscience Programme, Champalimaud Centre for the Unknown, Avenida Brasilia, 1400-038 Lisboa, Portugal*

[3] *UCL Ear Institute, University College London, 332 Gray's Inn Road, London, WC1X 8EE, UK*

[4] *Current address: Centre for Integrative Physiology and MRC Centre for Regenerative Medicine, School of Biological Sciences, University of Edinburgh, Edinburgh, UK.*

***Corresponding author**

Instituto de Medicina Molecular, Faculdade de Medicina de Lisboa, Portugal

Av. Professor Egas Moniz

1649-028 Lisboa, Portugal

E-mail: henrique@medicina.ulisboa.pt

Abstract

Mechanosensory hair cells (HCs) are the primary receptors of our senses of hearing and balance. Elucidation of the transcriptional networks regulating HC fate determination and differentiation is crucial not only to understand inner ear development but also to improve cell-replacement therapies for hearing disorders. Here, we show that combined expression of three transcription factors, Gfi1, Pou4f3 and Atoh1, can induce direct programming towards HC fate, both during *in vitro* embryonic stem cell (ESC) differentiation, and following ectopic expression in embryonic otic epithelium. Induced HCs (iHCs) express numerous HC-specific markers and exhibit polarized membrane protrusions reminiscent of stereociliary bundles. Transcriptome profiling confirms the progressive establishment of a HC gene specific signature during *in vitro* iHC programming. Overall, this work provides a novel approach to achieve robust and highly efficient HC production *in vitro*, which could be used as a model to study HC development and to drive inner ear HC regeneration.

Introduction

Sensory hair cells (HCs) of the inner ear are remarkable mechanoreceptors that convert the displacements of their specialized apical "hair" bundle into electrochemical signals. The mammalian inner ear has a very limited capacity to replace lost or damaged HC (Warchol, 2011), leading to permanent hearing and vestibular impairments for millions of people worldwide. Progress into the understanding of the transcriptional networks involved in HC fate specification has led to new therapeutic strategies for their replacement by gene or stem cell therapies. The basic helix-loop-helix (bHLH) transcription factor (TF) Atoh1 has received much attention because it has a key role in HC differentiation. *Atoh1* deletion in mice causes HC loss in all inner ear sensory organs (Bermingham et al., 1999; Cai et al., 2013), while its overexpression promotes the generation of ectopic HCs in the developing inner ear (Zheng and Gao, 2000; Woods et al., 2004; Kelly et al., 2012; Liu et al., 2012). However, *Atoh1* is also necessary for the specification of various subsets of neurons (Ben-Arie et al., 1997; Bermingham et al., 2001; Rose et al., 2009), intestinal secretory cells (Yang et al., 2001) and Merkel cells (Maricich et al., 2009), implying that Atoh1 acts in combination with different TFs to activate lineage-specific differentiation programs.

Besides Atoh1, the zinc-finger TF Gfi1 and the POU-domain TF Pou4f3 are the only known transcriptional regulators essential for proper differentiation and/or survival of all vestibular and auditory HCs (Xiang et al., 1997; Xiang et al., 1998; Wallis et al., 2003). The expression of *Gfi1* and *Pou4f3* is initiated in nascent HCs soon after the onset of *Atoh1* up-regulation (Wallis et al., 2003; Sage et al., 2006;

Pan et al., 2012). These findings raise the hypothesis that Gfi1 and Pou4f3 function together with Atoh1 in determining HC fate in the inner ear.

Previous reports have described relatively complex protocols that are able to steer ESC differentiation towards HC fate by recapitulating *in vivo* HC development through the temporal control of defined signaling pathways (Oshima et al., 2010; Koehler et al., 2013). Although stepwise differentiation protocols can promote successful HC generation *in vitro*, the efficiency of HC production is relatively low and reproducibility is a potential issue. This limits the use of these methods for inner ear studies where large cell numbers are needed, such as high-throughput drug screenings or cell transplantation therapies. Here, we report a simple, relatively quick and highly efficient protocol to generate sensory HCs *in vitro* from mouse ESCs (mESCs) by simultaneous overexpression of Gfi1, Pou4f3 and Atoh1.

Results

In vitro differentiation of mESCs into HC-like cells

To determine whether Atoh1 or the combination of Gfi1, Pou4f3 and Atoh1 TFs (GPA) can program mESC-derived progenitors into HCs, we first generated two mESC lines (iAtoh1 and iGPA) that enable doxycycline (Dox) inducible expression of these TFs (Kyba et al., 2002). The iGPA line contains a polycistronic cassette in which Gfi1, Pou4f3 and Atoh1 are linked by 2A peptides (Fig. 1A; and Supplementary material Fig. S1A,B), to allow robust and balanced co-expression of all three TFs upon Dox addition (Supplementary material Fig. S1C-F). In the absence of Dox, no significant expression of the inducible TFs was observed at the mRNA or protein level, while Dox treatment led to transgene expression in more than 60% of EB cells (Supplementary material Fig. S1C-F). We next subjected the iAtoh1 and iGPA mESCs to an embryoid body (EB)-mediated differentiation protocol in which Dox treatment was initiated at day 4 and maintained during the following 4 days, until day 8, when EBs were collected for analysis (Fig. 1B). Immunostaining for a HC marker, Myo7a (el-Amraoui et al., 1996), revealed striking differences between iAtoh1 and iGPA cells. Widespread up-regulation of Myo7a was only detected in iGPA-derived EBs (54 ± 2% of cells), and never in EBs originated from iAtoh1 cells, or in the absence of Dox (Fig. 1C-F). This suggests that the combined activities of the 3 TFs favor commitment towards HC fate. To investigate further the identity of induced Myo7a$^+$ (iMyo7a$^+$) cells in iGPA-derived EBs, we examined the expression of different markers known to be expressed at the onset of vestibular and auditory HC differentiation, such as Sox2, Lhx3 and Myo6 (Xiang et al., 1998; Hume et al., 2007). Notably, all iMyo7a$^+$ cells were found to co-express these markers (Fig. 1G-I). Quantitative reverse transcriptase PCR

(qRT-PCR) analyses also confirmed the significant increase of their transcript levels, compared to untreated EBs (Fig. 1K). In contrast, forced expression of Atoh1 alone in iAtoh1-EBs never resulted in up-regulation of HC markers (including Gfi1, Pou4f3 and hair bundle markers) (Supplementary material Fig. S2A-F). We have also tested whether forced Atoh1 expression might lead to cell death, as implied by (Liu et al., 2012). Given the known role of Gfi1 and Pou4f3 in promoting cell survival, their activity might counteract Atoh1 function and contribute to the differences in HC induction between iATOH1 and iGPA EBs. However, no significant differences were found in the percentage of apoptotic cells between iATOH1^{+} and iGPA^{+} cells (Supplementary material Fig. S3A-D), indicating that sustained expression of any of these TFs has no effect on the overall level of cell death in EBs, and that their differing effects in terms of HC induction are unlikely to be secondary to a different impact on cell viability.

During inner ear development, Sox2 expression rapidly declines as HC differentiation progresses (Hume et al., 2007). Thus, the strong Sox2 up-regulation we observed in iMyo7a^{+} cells suggests that these are at an initial phase of HC commitment. To assess their developmental status further, we next tested whether iMyo7a^{+} cells are already post-mitotic, as sensory progenitors first exit the cell cycle before initiating full differentiation as HCs (Ruben, 1967; Matei, et al., 2005; Chen et al., 2002). A 30 minute pulse of 5-ethynyl-2'-deoxyuridine (EdU) incorporation was performed 4 days after initiating Dox treatment in iGPA-derived EBs. Immunodetection revealed a clear lack of co-localization between EdU^{+} and iMyo7a^{+} cells, indicating that induced cells have already exited the cell cycle by this stage (Fig. 1J). Altogether, these observations suggest that co-expression of Gfi1, Pou4f3 and Atoh1 induces a rapid conversion of EB cells into postmitotic cells with

sensory HC characteristics, which we thereafter refer to as induced hair-cell-like cells, or iHCs.

Previous studies have shown that Gfi1, Pou4f3 and Atoh1 are also expressed during development of the central and peripheral nervous systems (Ninkina et al., 1993; Xiang et al., 1995; Ben-Arie et al., 2000; Wallis et al., 2003), and that each of these TFs is necessary for proper differentiation of multiple neuronal cell types (Ben-Arie et al., 1997; Bermingham et al., 2001; Wang et al., 2002; Tsuda et al., 2005; Rose et al., 2009). We therefore tested whether expression of the three TFs, or of Atoh1 alone, might also promote neuronal differentiation during EB differentiation, by examining the expression of neuronal marker Tuj1 and neural progenitor marker Nestin, which are not expressed in mammalian HCs (Malgrange et al., 2002; Wallis et al., 2003). We found that iGPA-derived EBs treated with Dox during 4 days do not exhibit any increase of either Tuj1 or Nestin expression (Supplementary material Fig. S2G,H). In contrast, iAtoh1-derived EBs show strong Tuj1 expression in most Atoh1-overexpressing cells (Supplementary material Fig. S2G). The absence of Nestin expression in iAtoh1-derived EBs (Supplementary material Fig. S2H) suggest that Atoh1 promotes direct conversion into neurons rather than inducing neural progenitors. These observations are consistent with previous in vivo studies showing that Atoh1 overexpression is sufficient to promote neural differentiation in nonneural ectoderm progenitors (Kim et al., 1997). Together, these results indicate that whilst Atoh1 is able to convert EB cells into neurons, the combination of Atoh1, Gfi1 and Pou4f3 drives progression towards a HC fate.

iHC-generation is enhanced by retinoic acid or inhibition of Notch signalling

In the embryo, HC differentiation is regulated by the Notch and retinoic acid (RA) signaling pathways, which can be manipulated to cause an increase in HC production: disruption of Notch signaling with gamma-secretase inhibitors leads to the overproduction of HCs at the expense of SCs (Kiernan, 2013), while RA supplementation of cultures of otic vesicles and sensory explants promotes the generation of extra HCs (Represa et al., 1990; Kelley et al., 1993). Hence, we decided to test if the efficiency of GPA-induced HC programming could be enhanced in a similar way. We exposed iGPA-derived EBs to 4 days of Dox treatment combined with either the gamma-secretase inhibitor LY411575 or RA (Fig. 2A). Remarkably, we found that the proportion of iHCs is significantly increased in presence of LY411575 (70 ± 2%) or RA (84 ± 1%), when compared to the Dox treatment alone (54 ± 2%) (Fig. 2B,C). In addition, mRNA expression levels of *Myo7a*, *Sox2*, *Myo6* and *Lhx3* are significantly elevated by RA-treatment of iGPA EBs (Fig. 2D), confirming that RA enhances HC programming efficiency. We have also examined the expression of *Nestin* and *Tubb3*, as neuronal commitment can occur upon RA treatment in differentiating EBs (Li et al., 1998). However, no significant up-regulation of either of these neural markers was detected (Fig. 2D), suggesting that the effect of RA on HC differentiation is quite specific.

iHCs are able to develop hair bundle-like structures

To determine whether iHCs are capable of developing stereociliary bundles similar to those of sensory HCs *in vivo*, we examined the expression of Espin, one of the

major actin-bundling proteins of stereocilia (Zheng, L. L. et al., 2000), in iGPA-derived EBs (Fig. 3A-C'). Immunostaining revealed weak Espin expression within GPA-expressing cells at day 8, after 4 days of Dox treatment (Fig. 3B). However, it is known that the onset of Espin expression during normal inner ear development occurs later than Myo7a (Chen et al., 2002; Sekerkova et al., 2006), raising the possibility that day 8 iHCs were still at an initial stage of HC differentiation. We therefore extended the period of Dox treatment for an additional 4 days, and examined EBs at day 12 (Fig. 3C). Notably, at this later time point, high levels of Espin are present in polarized membrane projections emanating from iHCs (Fig. 3C). These Espin-rich protrusions were observed in 55 ± 3% of Myo7a positive cells, a percentage that was not increased by RA treatment (55 ± 6%). Another essential hair bundle protein, Cadherin 23 (Cdh23) (Siemens et al., 2004), was also detected in the iHC-protrusions at day 12 (Supplementary material Fig. S4A). A significant increase in the expression of *Espin* and *Cadh23* at day 12 compared to day 8 was also found by qRT-PCR (Fig. 3D). The concurrent decline of Sox2 levels in iHCs between day 8 and day 12 (Fig. 3D; Supplementary material Fig. S4C) further supports the idea that iHCs progress towards a more mature HC phenotype (Fritzsch et al., 2014). We noticed that the Espin-rich protrusions in iHCs show heterogenous morphology and, although apparently polarized, do not exhibit consistent orientation (Fig. 3C'). We therefore hypothesized that exposing iHCs to inner ear polarity cues might improve the morphological differentiation of their hair bundle-like structures (Oshima et al., 2010). To test this idea, we established a co-culture system in which iGPA-derived EBs were dissociated and plated on the surface of mitotically inactivated utricle mesenchymal cells for 6 days, in the presence of Dox + RA (Fig. 3E). Although we could not observe a clear epithelial

organization with defined polarity among iHCs in these co-cultures, detailed confocal analysis revealed that the Espin-rich projections are preferentially directed towards either the bottom or the top of the cell layer (Fig. 3F-I; Supplementary material Fig. S4B). In addition, actin filaments are also present in these Espin-rich protusions (Fig. 3J), resembling normal HC stereocilia that contains a core of uniformly spaced actin filaments cross-linked with Espin.

In agreement with the immunostaining data, scanning electron microscopy shows that elongated membrane protrusions reminiscent of hair bundles are present at the apical surface of some iHCs (Fig. 3K). However, the vast majority of these putative bundles are poorly organized compared to normal HC stereociliary bundles, indicating that maturation of hair bundle-like structures in iHCs is incomplete under these culture conditions.

Combined expression of Gfi1-Pou4f3-Atoh1 can induce HC specification and differentiation *in vivo*

The lack of proper hair bundle maturation in iHCs could be due to inappropriate culture conditions, but it may also result from incomplete implementation of a HC-differentiation program by Gfi1, Pou4f3 and Atoh1. To address this question, we tested the effects of combined GPA expression *in vivo*, in the developing inner ear of chicken embryos, using a Tet-on inducible Tol2 transposon system that allows spatial and temporal control of transgene expression (Takahashi et al., 2008; Freeman et al., 2012). The otic cup was co-electroporated in ovo, at E2, with the TRE:GPA-eGFP vector (containing a bidirectional tetracycline-responsive element (TRE) that drives the expression of both Gfi1-Pou3f4-Atoh1 and eGFP upon Dox treatment), and plasmids encoding the rtTA-M2 tet-on activator and

Tol2 transposase (Fig. 4A). Two days later, embryos were treated with Dox and incubated for a further 2-4 days, until analysis at E6 or E8 (Fig. 4B). The results show that combined activity of Gfi1, Pou4f3 and Atoh1 induces Myo7a expression in electroporated cells located in various regions of the developing inner ear (n= 14/14 embryos, Fig. 4C,D), including both sensory and non-sensory domains of the vestibular and auditory system. Ectopic Myo7a$^+$ cells could even be found in the epithelium of the endolymphatic duct (a nonsensory component of the endolymphatic system, Fig. 4F). Among eGFP$^+$ cells analyzed at E6 in the vestibular and auditory regions, 77 ± 2% (n=265) and 76 ± 6% (n=492) showed Myo7a expression, respectively (4 independent inner ear samples were analyzed at E6). These ectopic Myo7a$^+$ cells are found preferentially located close to the luminal surface of the otic epithelium where HCs normally reside, and express other HC markers such as Sox2, Myo6, HCA (Hair Cell Antigen), Otoferlin (HCS-1) and Parvalbumin (Fig. 4E-K). They are also correctly polarized, with HCA-positive stereociliary bundles at the luminal surface (Fig. 4H',I). The production of HC is delayed in the auditory epithelium compared to the vestibular organs, and HC markers such as Myo7a, Myo6, HCA and HCS-1, are not yet detected in the basilar papilla at E6 (data not shown). Still, ectopic eGFP$^+$ iHCs located in the sensory and non-sensory regions of the cochlear duct express these HC markers already at E6 (Fig. 4H-J), suggesting that GPA expression can induce a fast commitment towards HC fate, independently of the developmental stage and character of the transfected cells. Remarkably, Tuj1-positive nerve fibers originating from the otic ganglia appear to be recruited by ectopic eGFP$^+$ HCs at E8, even when these cells are present in non-sensory epithelia (n=3/5, Fig. 4L). Altogether, these data show that

GPA expression can efficiently induce the generation of differentiated HCs from various type of otic progenitors *in vivo*.

Transcriptional profiling of iHCs reveals a specific HC signature

What is the precise genetic program induced by the combined activities of Gfi1, Pou4f3 and Atoh1, and to what extent does it match the transcriptional signature of a HC? To answer these questions, we first sought to obtain homogeneous populations of iHCs for transcriptional profiling. A novel iGPA-derived mESC line was prepared, containing a Myo7a promoter-driven fluorescence reporter system, to specifically label iHCs. This was based on an established *Myo7a* promoter, along with a strong HC-specific enhancer located in the intronic region 1 of *Myo7a*, which have been shown to drive specific transgene expression in vestibular and auditory HCs (Boeda et al., 2001). The new inducible reporter mESC line (iGPA-Myo7a:mVenus, Fig. 5A) showed comparable HC programming efficiency and RA sensitivity to the parental iGPA line (Fig. 5B). Although the Myo7a-reporter exhibited weak activity in the absence of induction (Fig. 5B,C,E), addition of Dox and RA led not only to a strong increase in the total number of Venus$^+$ cells, but also to much higher fluorescence levels per cell (Fig. 5B-D,F). Furthermore, a high degree of correlation between Venus and Myo7a expression was observed in these EBs, by immunostaining or by flow cytometry analysis following intracellular antibody staining (Fig. 5F). These results indicate that the Myo7a:mVenus reporter provides an effective read-out for Myo7a-induction during HC programming. We next used the iGPA-Myo7a:mVenus reporter line and FACS to isolate day 8 and day 12 iHCs from EBs that were treated with either Dox alone or with Dox and RA. Unsorted EBs from the same reporter line, grown in the same conditions but

without Dox or RA treatment, were used as controls. Independent RNA preparations from each of the selected time points and treatments (three biological replicates for Dox or Dox+RA treatments, two for "no treatment") were processed and hybridized on Affymetrix whole-transcript microarrays (Mouse Genome 2.1 ST Arrays Strip).

Hierarchical clustering of the transcriptome datasets reveals a clear segregation between "No Dox" and "Dox" samples (Fig. 6A). Interestingly, in the Dox branch, samples cluster in two groups: one containing day 8 iHCs treated with Dox, and the other composed of day 8 iHCs treated with Dox + RA, together with all the day 12 iHCs samples (Fig. 6A). This suggests that day 8 iHCs treated with RA reach a differentiation stage similar to that of day 12 iHCs, indicating that RA treatment improves the efficiency of iHC programming by accelerating progression towards a more mature HC state. This would be consistent with the earlier onset of Myo7a expression in RA-treated iGPA EBs (Supplementary material Fig. S5A-C).

We next analyzed the genes differentially expressed in iHC populations obtained with different treatments, by comparison with control ("no Dox") cells at the same time point (Supplementary material Table S1). Enrichment of gene ontology (GO) functional groups for up-regulated genes in day 8 iHCs was found to be related with neuronal differentiation and inner ear development (Fig. 6B,C). On the other hand, the set of up-regulated genes in day 12 iHCs is highly enriched in genes involved in inner ear development and HC functions, such as sensory perception of sound/mechanical stimulus and synaptic transmission (Fig. 6D,E). Strikingly, analysis of the subset of day 8 up-regulated genes that are further up-regulated at day 12 reveals a stronger enrichment in gene categories involved in HC functions (Fig. 6F,G). Furthermore, GO analysis shows that genes connected to the cell cycle

and cell division are specifically repressed in iHCs (Supplementary material Fig. S6A-D), consistent with the observation that these cells have ceased proliferation and exited cell cycle. Altogether, this analysis indicates that the combined activity of Gfi1, Pou4f3 and Atoh1 is able to induce a bona fide HC developmental program. This conclusion is also supported by the significant overlap between the transcriptional profiles of iHCs and Atoh1-GFP sorted HC populations from P1 mouse cochleas: out of a core HC signature of 500 genes defined for Atoh1-GFP HCs (T. Cai and A. Groves, personal communication), 69% are upregulated in iHCs (Fig. 6H). In contrast, only 38% of the defined Atoh1 gene targets in cerebellar granule neuron precursors (CGPs) (Klisch et al., 2011) are up-regulated in iHCs (Fig. 6I).

Finally, we analysed the transcriptome datasets for the expression of genes known to be functionally relevant for inner ear HC development/function. We first selected a list of 250 genes associated to hereditary forms of deafness in mouse or humans (http://hearingimpairment.jax.org/master_table.html), and further refined this gene set by selecting those that are known to be expressed in HCs (Supplementary material Table S1, 88 genes) Analysis of their expression in iHCs at different stages shows that the majority of these 88 genes are significantly up-regulated by the combined activity of the 3 TFs, in particular in day 12 iHCs, which exhibit a clear enrichment in expression of deafness genes known to participate in the formation of hair bundles (Fig. 6J,K).

Since multiple genes involved in the mechanoreception machinery are expressed in iHCs, we asked whether functional mechanotransduction channels are also present in these cells, by performing a FM1-43 permeation assay (Gale et al., 2001). When co-cultures grown in the absence of Dox were exposed (sixty

seconds) to FM1-43, no labelled live cells were detected (Supplementary material Fig. S7A). In contrast, in Dox treated cells (day 12 with RA), around 25% of the Venus$^+$ population was labelled by FM1-43 (Supplementary material Fig. S7B). The specific internalisation of FM1-43 into Venus$^+$ cells suggests that these cells contain open and potentially functional mechanotransduction channels.

Discussion

We report here that a combination of three TFs (Gfi1, Pou4f3 and Atoh1) is able to promote the direct conversion of somatic cells into HC-like cells, both *in vitro* and *in vivo*. Transcriptome profiling of iHCs at different stages reveals that a specific HC genetic program is activated in these cells. This program appears to recapitulate normal progression of HC development: genes that are induced early (day 8) are known to participate in HC commitment, while genes encoding components of the mechanotransduction machinery are activated at a later stage of the process (day 12), coinciding with the appearance of polarized espin-rich hair bundle-like protrusions in iHCs. Although these bundles are less organized than native stereociliary bundles, some iHCs are able to rapidly incorporate the FMI-43 dye, consistent with the presence of functional mechanoreceptor channels in these cells. Altogether, our data suggests Gfi1, Pou4f3 and Atoh1 can activate the HC genetic program required for the specification and differentiation of functional HCs. However, proper maturation of iHCs is likely to be dependent on additional extrinsic and intrinsic cues.

A combinatorial transcriptional control for hair cell formation

Our results show that Gfi1, Pou4f3 and Atoh1 are core TFs of the genetic network regulating HC differentiation. Although Atoh1 has been considered a "master" gene for HC differentiation, due to its capacity to induce new HCs following ectopic expression in the inner ear (Zheng and Gao, 2000; Woods et al., 2004), our work shows that this pro-HC function is context dependent, as Atoh1 is unable to induce a HC fate in EB cells, driving instead a neuronal differentiation program. In contrast, we show here that the combination of Atoh1 with Gfi1 and Pou4f3 leads

to the implementation of a HC differentiation program in EB cells, as well as in the non-sensory otic epithelia. These findings unveil a novel regulatory layer on HC fate specification, and provide a molecular basis to explain how Atoh1 can induce different cell fates in the embryo, not only HCs in the inner ear, but also Merkel cells in the skin, secretory cells in the intestine or granule neurons in the cerebellum (Mulvaney and Dabdoub, 2012).

A pertinent question is therefore what roles Gfi1 and Pou4f3 play in this process. Gfi1 is a known transcriptional repressor and previous studies indicate that it might contribute to divert Atoh1-expressing cells from an exclusively neural differentiation program. For instance, HCs in the inner ears of *Gfi1* mutant mice exhibit abnormal Tuj1 expression, suggesting a partial transformation into neurons (Wallis et al., 2003). Also, in the intestinal epithelium of *Gfi1*-null mice, Atoh1-dependent mucous and Paneth cells acquire abnormal Ngn3 expression and can convert to pro-enteroendocrine lineages (Bjerknes and Cheng, 2010). However, Gfi1 may also act as a transcriptional coactivator to positively modulate Atoh1 activity, by analogy with the functional interaction between their *Drosophila* homologues (Senseless and Atonal) during sensory precursor specification (Jarman and Groves, 2013). In this process, Senseless may function to increase or modify Atonal's E-box binding specificity, modulating its proneural functions. Whether Senseless/Gfi1 acts by direct physical interaction with Atonal/Atoh1, or by binding promoter regions adjacent to E-boxes to modulate their proneural/pro-HC functions remains to be investigated. However, in the case of HC induction here discussed, it is unlikely that the observed specificity can be ascribed only to the modulatory activity of Gfi1, as the pair Atoh1/Gfi1 is also active during other cell

fate decision processes, like the determination of secretory cell identities in the intestinal crypts (Shroyer et al., 2005; Bjerknes and Cheng, 2010).

Although we have not tested whether Pou4f3 is absolutely required for HC induction in EBs, it is likely that this TF plays also an essential role in the process, not only by independently activating an additional set of HC differentiation genes, but also by modulating Atoh1/Gfi1 activity to establish a specific HC genetic program. The first function is suggested by the critical role of Pou4f3 in ensuring proper differentiation and survival of all vestibular and auditory HCs (Xiang et al., 1998). The second role of Pou4f3 in contributing to the specificity of Atoh1/Gfi1 driven HC induction is suggested by the observed cooperation between Pou3f2, a related member of the Pou-HD family of TFs, and the bHLH TF Ascl1, to activate a neurogenic program in the developing mouse CNS (Castro et al., 2006).

We should also note the remarkable similarity between the cocktail of TFs used to convert fibroblasts and hepatocytes into neurons (Ascl1, Brn2 and Myt1l) (Vierbuchen et al., 2010; Marro et al., 2011) and the three TFs used in our study, in both cases consisting of a bHLH TF, a Pou-HD TF and a Zinc-Finger TF. However, whereas the main contribution of Brn2 and Myt1l is to increase Ascl1's neuronal reprogramming efficiency, our results show that Gfi1 and Pou4f3 are able to radically alter the Atoh1 transcriptional program to promote a distinct HC-differentiation program. The work here described thus offers a new model system to address the crucial question of how similar sets of TFs can operate in different modes to implement unique cell fates.

Similarities and differences in the transcriptional profiles of iHCs and native HCs

The ability to obtain purified populations of iHCs using the Myo7:mVenus reporter line allowed us to generate highly reproducible gene expression profiles for these cells, at various phases of their differentiation. Comparison of the iHC transcriptional signature with a core gene expression signature defined for cochlear HCs (500 genes; T. Cai and A. Groves, personal communication) reveals that 69% of core HC genes are up-regulated by the combined activity of Gfi1, Pou4f3 and Atoh1 in iHCs. When these HC signatures are compared with the set of Atoh1 target genes in cerebellar granule neurons (Klisch et al., 2011), the overlap is much smaller (28% for cochlea HCs and 38% for iHCs), supporting the conclusion that Gfi1, Pou4f3 and Atoh1 activate a HC specific genetic program. This comparison highlights also the existence of a common set of Atoh1 targets between neurons and HCs, possibly underlying the similar capacity of these cell types to engage in neurotransmission.

The finding that 30% of core HC genes are not activated by the three TFs in iHCs correlates well with the relative immaturity of these cells in culture. Actually, amongst the ~30% of HC genes that are not up-regulated in iHCs, there are several "deafness" genes encoding late-expressed hair-bundle proteins, such as Slc9a9, Fscn2, Gpr98, Myo3a and Strc. It is possible that the lack of expression of these genes is due to a developmental delay, as day 12 iHCs (8 days after induction of the 3 TFs) are likely to be less advanced in development than the P1 cochlear Atoh1-GFP cells used to define a core HC signature. Another reason might be that the GPA combination can only induce a partial HC phenotype, lacking the activity of additional TFs that are crucial for late HC differentiation. By comparison with the Atonal-driven sensory program in *Drosophila* Chordotonal (Ch) neurons (Newton et al., 2012) in which the TF Fd3F acts downstream of Atonal to regulate various

genes required for assembly of mechanosensory cilia, we noticed that various "missing" iHC genes are homologs of Fd3F targets in *Drosophila*. These include *Tekt1*, *Wdr63*, *Dnahc6*, *Dnahc9* and *Dynlrb2*, all involved in axonemal dynein assembly. These genes are also known to be direct or indirect targets for the vertebrate homolog of Fd3F - Foxj1 (Stubbs et al., 2008; Jacquet et al., 2009). However, Foxj1 is induced in iHCs by the GPA combination, suggesting that the absent expression of its targets is due to a blockage of its activity in immature iHCs, preventing for instance the formation of a proper kinocilium. We have also scrutinized the list of Atoh1 neuronal targets that are repressed in iHCs, and two genes are worth mentioning, Gli2 and FoxM1, which are known to be crucial for Shh-driven proliferation of cerebellar granule neuron precursors (CGPs) (Flora et al., 2009). Repression of these genes in iHCs illustrates how the combination of Atoh1 with Gfi1 and Pou4f3 leads to key differences in gene expression, with likely functional consequences: while Atoh1 induction of Gli2 in CGPs allows these cells to proliferate in response to Shh (Flora et al., 2009), Gli2 repression in iHCs might shield these cells from Shh and contribute to the fast cell cycle exit that we observed after induction of the 3 TFs.

Maturation of iHC *in vitro* requires an adequate cellular environment

Despite their clear progression towards HC differentiation, iHCs failed to develop stereotypical hair bundles *in vitro*. The morphology and length of the espin-rich projections of iHCs were heterogeneous, and although clearly polarized, their position and orientation were variable. This could be due to the inability of iHCs to form a coherent epithelium in culture, preventing the definition of apical-basal polarity required for hair bundle differentiation. In contrast, overexpression of

Gfi1, Pou4f3 and Atoh1 in the embryonic chick inner ear induced ectopic but normally polarized HCs, indicating that this TF combination does not interfere with normal progression of HC differentiation. These findings thus suggest that environmental factors and/or a proper cellular context are essential to achieve complete *in vitro* HC differentiation. Concerning the first, our data shows that inhibition of Notch signaling or addition of RA can improve iHC differentiation. Notch activity is known to prevent HC specification in the inner ear (Kiernan, 2013), and our microarray data reveals that Notch signaling is active during iHC formation (Supplementary material Fig. S8). Addition of a Notch inhibitor is therefore expected to facilitate iHC formation, and our results confirm this. The activity of RA was also expected to increase iHC differentiation, following previous findings that addition of RA to chick otic vesicles or mouse organ of Corti explants results in early onset of HC differentiation and supernumerary HCs (Represa et al., 1990; Kelley et al., 1993). Little is known about how RA signaling leads to this effect, and our work might offer some cues on the underlying molecular mechanisms. For instance, the finding that RA addition represses Hes1 expression raises the hypothesis that this could relieve Atoh1 from its antagonizing activity (Zheng, J. L. et al., 2000) and lead to an increased efficiency of iHC generation.

Concerning the requirement for an adequate multicellular organization for iHC differentiation, we have used several strategies to address this issue, either by co-culturing iHCs with otic-derived mesenchymal cells or by using various synthetic scaffolds to grow dissociated EB cells, but never observed a proper epithelial organization of iHC aggregates *in vitro*. A possible explanation is the absence of supporting cells (SCs) in iHC cultures, which are necessary *in vivo* to establish specific cell-cell adhesion with HCs. In fact, our data suggest that GPA induction of

iHCs does not lead to the concomitant induction of SCs. Although iHCs expressed Sox2, typical supporting cell markers such as Prox1 and E-cadherin were absent in Dox-treated EBs (data not shown), and analysis of iHC transcriptomes confirms the lack of expression of SC genes (GFAP, neurotrophin receptor P75, GLAST, and Jag1). This suggests that the combined activation of Gfi1, Pou4f3 and Atoh1 promotes a direct conversion into a HC fate, bypassing the bipotent progenitor cell state that normally precedes SC and HC formation *in vivo*.

In summary, we report here the first successful and efficient method for direct conversion of mESC-derived progenitors into iHCs, providing a proof-of-concept for HC programming. This simple and rapid method offers an alternative approach to produce large numbers of HC-like cells *in vitro*. Further work shall be aimed at investigating whether forced expression of Gfi1-Pou4f3-Atoh1 could also direct other somatic cell types towards HC differentiation, and how these three TFs regulate HC commitment and differentiation.

Methods

ESC maintenance and differentiation

Ainv15, iAtoh1, iGPA and iGPA-Myo7a:mVenus mESC lines were maintained on gelatin-coated dishes in DMEM (Invitrogen) supplemented with 10% ES-qualified FBS (Invitrogen), 1 mM 2-mercaptoethanol and 2 ng/ml LIF. For EB differentiation, mESCs were trypsinized using 0.25% trypsin-EDTA (Invitrogen) and re-suspended on bacterial-grade Petri dishes in the same medium without LIF. Medium supplementation with 2 μg/ml Dox, 1 μM RA and 10 nM LY411575 was performed as described in figures.

Generation of iAtoh1 and iGPA lines

Ainv15 mESC cells ($4x10^6$) were electroporated (Gene Pulser II, Bio-Rad; 250 V,500 μF) with 20 μg of pTurbo-Cre and 20 μg of Atoh1Plox or GPAPlox vectors (see supplemental experimental procedures). Cells were subsequently plated on neomycin-resistant and mitotically inactivated MEF feeders cells in DMEM medium supplemented with 350 μg/ml of G418. Individual colonies were picked 10–14 days after electroporation.

RNA extraction, quantitative PCR and Microarray analysis

Total RNA was extracted from 10^6 EB-derived cells subjected to different culture conditions using High Pure RNA Isolation kit (Roche Diagnostics) according to for hybridization on Mouse Genome 2.1 ST Arrays Strip (Affymetrix). Log2 expression values of the several transcripts were imported to Chipster 2.4 for data analysis. To perform quantitative real-time PCR, first strand cDNA was synthesized from 1 μg of total RNA using SuperscriptII Reverse Transcriptase (Invitrogen) and random

hexamers. Real-time PCR was performed with SYBR green and exon spanning primers in 7500 and ViiA 7 Real-Time PCR systems (Applied Biosystems).

Chicken otic cup electroporation

Electroporations of the inner ear was performed at E2 using Electro Square PoratorTM ECM830 (BTX) as described in (Freeman et al., 2012). The Tol2 transposon vectors were electroporated at a final concentration of 1 µg/µl.

Statistics

All data are expressed as mean ± standard error of mean (SEM) and statistical significance was assessed using an unpaired Student's *t*-test. For all statistics, data from at least 3 biologically independent experiments were used. Data and graphs were tabulated and prepared using Microsoft Excel and GraphPad Prism software. Statistically significant differences are indicated as follows:*P<0,05 **P<0,01 ***P<0,001

Author Contributions

A.C. conceived, performed and analyzed the experiments, wrote the paper. L.S-G. performed the chick electroporations. S.J. prepared the inactivated utricle periodic mesenchyme cells. J.G. and N.D. provided scientific and technical advice for some experiments. D.H. conceived and supervised the study, wrote the paper.

Acknowledgments

We thank Tiantian Cai and Andrew Groves for sharing unpublished RNA-seq data from ATOH1:GFP HCs. Jörg Becker/IGC gene exp. Unit for technical support with microarray analysis. Andrew Forge and Telmo Nunes for SEM support. Sara Ferreira, IMM bioimaging and flow cytometry facilities for technical help. Fernando Giraldez for critical reading of the manuscript. Filipe Vilas-Boas for helpful discussions.

This work was supported by Fundação para a Ciência e Tecnologia, Portugal (PTDC/SAU-NEU/71310/2006, SFRH/BD/38461/2007 to AC). AC was also a recipient of an EMBO Short-term Fellowship during her stay at the Ear Institute.

Accession number

The GEO accession number for the mRNA microarray data is GSE60352.

Competing financial interests

The authors declare no competing financial interests

Figure Legends

Fig. 1.

Inducible expression of Gfi1-Pou4f3-Atoh1 promotes the differentiation of EB-derived progenitors towards HC fate

(A) Schematic representation of Dox-inducible iAtoh1 and iGPA lines used in this paper.

(B) Schematic diagram of mESC differentiation protocol describing the Dox treatment timeline.

(C) Graph showing the mean percentage of Atoh1^{+} cells that are positive for Myo7a in iGPA and iAtoh1 cells, after 4 days of Dox treatment.

(D-F) Immunostaining analysis of Myo7a and Atoh1 expression in EBs harvested at day 8 from the iAtoh1 mESC line (D) and iGPA line (E and F). Strong upregulation of Myo7a is detected only in iGPA-derived Atoh1^{+} cells (E).

(G-I) Representative images obtained from immunostaining for Myo7a/Sox2 (G), Myo7a/Lhx3 (H), Myo7a/Myo6 (I), and Myo7a/EdU (J), of iGPA EBs, analyzed at day 8, after 4 days of Dox exposure.

(K) Quantitative RT-PCR analysis reveals up-regulation of Myo7a, Sox2, Myo6 and Lhx3 in iGPA-derived EBs treated for 4 days with Dox. Relative expression of each transcript is presented as fold change normalized to the mean of untreated EBs (dotted baseline = 1) at day 8.

Results are mean ± SEM. $^{**}P<0,01$ $^{***}P<0,001$ (n=3); 2AP, 2A peptide; TRE, tetracycline responsive element; rtTA, reverse tetracycline transactivator.

Fig. 2.

Enhancing the HC programming efficiency by Notch inhibition or RA exposure

(A) Schematic diagram of iGPA EB differentiation protocols, including the combinatorial treatment of Dox plus LY411575 or RA.

(B) Quantification of Myo7a$^+$ cells found among cells expressing the 3 TFs (Pou4f3$^+$ cells) analysed in 8 day EBs treated with Dox, Dox + LY411575 and Dox + RA.

(C) Representative images of iGPA-derived EBs at day 8, obtained by immunostaining of Pou4f3 and Myo7a, showing significant increase of Myo7a$^+$ cells by combined treatment of Dox+LY411575 or Dox+RA, compared to Dox treatment alone.

(D) Quantitative RT-PCR analysis shows higher expression levels of HC markers (*Myo7a*, *Sox2*, *Myo6* and *Lhx3*), but not neuronal markers (*Nestin* and *Tubb3*), in EBs treated with Dox + RA compared to Dox treatment. Fold change was normalized to the mean of untreated EBs (dotted baseline = 1).

Results are mean ± SEM. **P*<0,05 ***P*<0,01 ****P*<0,001 (n=3). RA, retinoic acid.

Fig. 3.

Morphological characterization of hair bundle-like structures in iHCs

(A) Schematic diagram of iGPA EB differentiation protocol describing the Dox treatment timeline.

(B and C) Immunostaining for Espin and Myo7a in iGPA-derived EBs treated with Dox during 4 days (B) and 8 days (C) reveals a strong and polarized Espin+ structure on the surface of iMyo7a$^+$ cells. These structures were absent in EBs that had only 4 days of Dox exposure (B). Squares indicate areas of magnification for each time point represented on the right of the panel (B' and C').

(D) Bar diagram showing the relative mRNA levels (presented as fold change normalized to the mean of untreated EBs at the corresponding time point, dotted baseline = 1) of genes encoding hair bundle markers (*Espin* and *Cdh23*), HC markers (*Myo7a* and *Sox2*) and neuronal markers (*Nestin* and *Tubb3*) in EBs treated with Dox or Dox + RA, at day 8 and at day 12.

(E) Schematic diagram of dissociated EB co-culture differentiation protocol with mitotically inactivated chicken utricle periodic mesenchyme cells.

(F) Confocal stacks of hair bundle-like protrusions labelled with Myo7a and Espin, in the adherent co-cultures at day 12. Note that F' and F'' are orthogonal views showing Espin$^+$ structures oriented towards the utricle mesenchyme layer (arrow in F') or in the opposite direction facing the cell surface (arrowhead in F'').

(G-J) Confocal images showing representative Espin$^+$ and Myo7a$^+$ protrusions in several iHCs grown in adherent co-cultures at day 12. Phalloidin immunostaining shows that polarized Myo7a$^+$/Espin$^+$ structures are F-actin-filled membrane protrusions (J).

(K) Morphology of microvilli-like stereocilia protruding from the cell surface of an iHC observed by scanning electron microscopy.

Results are mean ± SEM. *P<0,05 **P<0,01 ***P<0,001 (n=3).

Fig. 4.

Induction of Gfi1-Pou4f3-Atoh1 expression induces HC differentiation in various regions of the embryonic chick inner ear.

(A) Schematic diagrams of the expression vectors used for Dox-inducible Gfi1-Pou4f3-Atoh1 and eGFP expression by *in ovo* electroporation. Note that eGFP is fused with histone 2B (H2B) for nuclear localization.

(B) Experimental design to test the effects of Gfi1-Pou4f3-Atoh1 expression during inner ear development in the chick embryo.

(C and D) Representative images of the vestibular (C) and auditory epithelia (D) showing Myo7a and eGFP immunofluorescence in E6 electroporated embryos. Squares indicate areas of magnification represented on the right of the panel (C' and D').

(E) A section through the vestibular region shows electroporated eGFP$^+$ cells with Myo6 expression in various sensory patches (arrowheads), as well as in non-sensory domains of the otic epithelium (E'). Non-electroporated patches with Myo6-expressing HCs are also present (*).

(F and G) Immunostaining analysis for Myo7a/eGFP/Sox2 showing expression of Sox2 in ectopic Myo7a$^+$ cells (E' and F').

(H and I) Immunostaining analysis for Myo6/eGFP/HCA in the vestibular (H) and auditory epithelium (I) shows polarized localization of HCA in the apical domain of ectopic iHCs (red in H, white colored in I and H').

(J and K) Analysis of electroporated eGFP+ cells in the basilar papilla epithelium shows that ectopic iHCs express the HC markers otoferlin/HCS-1 (J) and Parvalbumin (K).

(L) Ectopic iHCs (expressing Myo6 and HCA) are innervated by Tuj1-positive neuronal extensions (arrowheads) that project from neurons at the otic ganglion. Some ectopic HCs are eGFP-negative, possibly due to eGFP decay at E8 (Dox was added only at E4).

bp, basilar papilla; cd, cochlear duct; lc, lateral crista; u, utriculi; s, sacculi; pc, posterior crista; mu, macula utriculi; ms, macula sacculi; ed, endolymphatic duct. Orientation: A, anterior; M, medial.

Fig. 5.

The iGPA-Myo7a:mVenus ES line is an adequate fluorescence reporter for Myo7a expression

(A) Schematic diagram of the iGPA-Myo7a:mVenus ES line containing the mouse Myo7a regulatory regions driving transcription of a Venus fluorescent protein, followed by a selection cassette.

(B) Quantification analysis of $Pou4f3^{+,}$ $Myo7a^{+}$ and $Venus^{+}$ cells relative to total cell numbers found within EBs grown in the absence or presence of Dox and Dox + RA at day 8. Cells counts were performed for EBs generated from the iGPA and iGPA:Myo7a:mVenus lines. No significant differences were found between these 2 lines regarding the mean percentage of total $Pou4f3^{+}$ and $Myo7a^{+}$ cells in the different treatments.

(C) Representative histogram showing Venus expression in iGPA:Myo7a:mVenus-derived EBs untreated (grey; 14,5 ± 0,4%), treated with Dox (orange; 46,9 ± 4,1%) and Dox + RA (blue; 46 ± 4,6%) at day 8.

(D) Brightfield and fluorescence images of live floating iGPA:Myo7a:mVenus-derived EBs at day 8, showing weak Venus fluorescence levels in the absence of Dox, but high numbers of strongly fluorescent Venus$^+$ cells following Dox induction.

(E and F) Immunostaining analysis for Myo7a and Venus in iGPA-Myo7a:mVenus-derived EBs, in untreated (E) or Dox +RA treated conditions (F) at day 8, showing a high degree of co-localization between the 2 proteins; (79,54 ± 0,34% and 54,39 ± 1,65% of Venus$^+$ cells were Myo7a$^+$ in EBs treated with Dox + RA and Dox, respectively). Included are representative dot plots of intracellular staining for Myo7a and Venus proteins, analysed by flow cytometry. Statistical analysis indicates a good correlation between the expression of both proteins (Pearson correlation = 0.601).

Results are mean ± SEM (n=3); PGK, phospho-glycero-kinase promoter; Blasticidine, blasticidine resistance gene; FC-IS, flow cytometry analysis following intracellular staining.

Fig. 6.

Analyses of iHC transcriptome profiles

(A) Dendrogram showing the hierarchical clustering of the various expression profiles obtained from iGPA-Myo7a:mVenus reporter-derived EBs (E1, E2 and E3 correspond to three biological replicates).

(B-E) Gene ontology analysis performed using the DAVID functional annotation tool for genes significantly up-regulated (fold change>2, *P*-value<0,01) in the four different iMyo7a:Venus groups, relative to uninduced cells. The number of up-regulated genes included in each GO functional term is shown.

(F and G) Venn diagram illustrating the overlap between the significantly up-regulated genes identified in iMyo7a^{+} cells at day 8 and day 12, compared with uninduced cells. From the list of common up-regulated genes in iGPA cells treated with Dox only, those that show higher fold change at day 12 were selected. This list was subjected to a GO analysis using the DAVID functional annotation tool. The same procedure was performed for the overlapping genes from iGPA cells cultured with Dox +RA (G).

(H) Heat map depicting the relative fold changes in expression of 500 core HC genes (T. Cai and A. Groves, personal communication) across the four different iMyo7a groups, relative to uninduced cells (*P*-value<0,05).

(I) Venn diagram illustrating the overlap between the transcriptome of cochlear core HC signature and iHCs (*P*-value<0,05) relative to the 601 cerebellum Atoh1 direct target genes previously identified in (Klisch et al., 2011).

(J and K) Heat maps depicting the relative fold changes in expression of deafness-related genes across the four different iMyo7a groups, relative to uninduced cells (*P*-value<0,05).

References:

Ben-Arie, N., Bellen, H. J., Armstrong, D. L., McCall, A. E., Gordadze, P. R., Guo, Q., Matzuk, M. M. and Zoghbi, H. Y. (1997). Math1 is essential for genesis of cerebellar granule neurons. *Nature* **390**, 169-172.

Ben-Arie, N., Hassan, B. A., Bermingham, N. A., Malicki, D. M., Armstrong, D., Matzuk, M., Bellen, H. J. and Zoghbi, H. Y. (2000). Functional conservation of atonal and Math1 in the CNS and PNS. *Development* **127**, 1039-1048.

Bermingham, N. A., Hassan, B. A., Wang, V. Y., Fernandez, M., Banfi, S., Bellen, H. J., Fritzsch, B. and Zoghbi, H. Y. (2001). Proprioceptor pathway development is dependent on MATH1. *Neuron* **30**, 411-422.

Bermingham, N. A., Hassan, B. A., Price, S. D., Vollrath, M. A., Ben-Arie, N., Eatock, R. A., Bellen, H. J., Lysakowski, A. and Zoghbi, H. Y. (1999). Math1: an essential gene for the generation of inner ear hair cells. *Science* **284**, 1837-1841.

Bjerknes, M. and Cheng, H. (2010). Cell Lineage metastability in Gfi1-deficient mouse intestinal epithelium. *Dev. Biol.* **345**, 49-63.

Boeda, B., Weil, D. and Petit, C. (2001). A specific promoter of the sensory cells of the inner ear defined by transgenesis. *Hum. Mol. Genet.* **10**, 1581-1589.

Cai, T., Seymour, M. L., Zhang, H., Pereira, F. A. and Groves, A. K. (2013). Conditional deletion of Atoh1 reveals distinct critical periods for survival and function of hair cells in the organ of Corti. *J. Neurosci.* **33**, 10110-10122.

Castro, D. S., Skowronska-Krawczyk, D., Armant, O., Donaldson, I. J., Parras, C., Hunt, C., Critchley, J. A., Nguyen, L., Gossler, A., Gottgens, B. et al. (2006). Proneural bHLH and Brn proteins coregulate a neurogenic program through cooperative binding to a conserved DNA motif. *Dev. Cell* **11**, 831-844.

Chen, P., Johnson, J. E., Zoghbi, H. Y. and Segil, N. (2002). The role of Math1 in inner ear development: Uncoupling the establishment of the sensory primordium from hair cell fate determination. *Development* **129**, 2495-2505.

Davies, S. and Forge, A. (1987). Preparation of the mammalian organ of Corti for scanning electron microscopy. *J. Microsc.* **147**, 89-101.

el-Amraoui, A., Sahly, I., Picaud, S., Sahel, J., Abitbol, M. and Petit, C. (1996). Human Usher 1B/mouse shaker-1: the retinal phenotype discrepancy explained by the presence/absence of myosin VIIA in the photoreceptor cells. *Hum. Mol. Genet.* **5**, 1171-1178.

Flora, A., Klisch, T. J., Schuster, G. and Zoghbi, H. Y. (2009). Deletion of Atoh1 disrupts Sonic Hedgehog signaling in the developing cerebellum and prevents medulloblastoma. *Science* **326**, 1424-1427.

Freeman, S., Chrysostomou, E., Kawakami, K., Takahashi, Y. and Daudet, N. (2012). Tol2-mediated gene transfer and in ovo electroporation of the otic placode: a powerful and versatile approach for investigating embryonic development and regeneration of the chicken inner ear. *Methods Mol. Biol.* **916**, 127-139.

Fritzsch, B., Jahan, I., Pan, N., Elliott, K. L. (2014). Evolving gene regulatory networks into cellular networks guiding adaptive behavior: an outline how single cells could have evolved into a centralized neurosensory system. *Cell Tissue Res.* **359**, 295-313.

Gale, J. E., Marcotti, W., Kennedy, H. J., Kros, C. J. and Richardson, G. P. (2001). FM1-43 dye behaves as a permeant blocker of the hair-cell mechanotransducer channel. *J. Neurosci.* **21**, 7013-7025.

Hume, C. R., Bratt, D. L. and Oesterle, E. C. (2007). Expression of LHX3 and SOX2 during mouse inner ear development. *Gene Expr. Patterns* **7**, 798-807.

Jacquet, B. V., Salinas-Mondragon, R., Liang, H. X., Therit, B., Buie, J. D., Dykstra, M., Campbell, K., Ostrowski, L. E., Brody, S. L. and Ghashghaei, H. T. (2009). FoxJ1-dependent gene expression is required for differentiation of radial glia into ependymal cells and a subset of astrocytes in the postnatal brain. *Development* **136**, 4021-4031.

Jarman, A. P. and Groves, A. K. (2013). The role of Atonal transcription factors in the development of mechanosensitive cells. *Semin. Cell Dev. Biol.* **24**, 438-447.

Kallio, M. A., Tuimala, J. T., Hupponen, T., Klemela, P., Gentile, M., Scheinin, I., Koski, M., Kaki, J. and Korpelainen, E. I. (2011). Chipster: user-friendly analysis software for microarray and other high-throughput data. *BMC genomics* **12**, 507.

Kelley, M. W., Xu, X. M., Wagner, M. A., Warchol, M. E. and Corwin, J. T. (1993). The developing organ of Corti contains retinoic acid and forms supernumerary hair cells in response to exogenous retinoic acid in culture. *Development* **119**, 1041-1053.

Kelly, M. C., Chang, Q., Pan, A., Lin, X. and Chen, P. (2012). Atoh1 directs the formation of sensory mosaics and induces cell proliferation in the postnatal mammalian cochlea in vivo. *J. Neurosci.* **32**, 6699-6710.

Kiernan, A. E. (2013). Notch signaling during cell fate determination in the inner ear. *Semin. Cell Dev. Biol.* **24**, 470-479.

Kim, P., Helms, A. W., Johnson, J. E. and Zimmerman, K. (1997). XATH- 1, a vertebrate homolog of Drosophila atonal, induces a neuronal differentiation within ectodermal progenitors. Dev. Biol. **187**, 1-12.

Klisch, T. J., Xi, Y. X., Flora, A., Wang, L. G., Li, W. and Zoghbi, H. Y. (2011). In vivo Atoh1 targetome reveals how a proneural transcription factor regulates cerebellar development. *Proc. Natl. Acad. Sci. USA* **108**, 3288-3293.

Koehler, K. R., Mikosz, A. M., Molosh, A. I., Patel, D. and Hashino, E. (2013). Generation of inner ear sensory epithelia from pluripotent stem cells in 3D culture. *Nature* **500**, 217-221.

Kyba, M., Perlingeiro, R. C. and Daley, G. Q. (2002). HoxB4 confers definitive lymphoid-myeloid engraftment potential on embryonic stem cell and yolk sac hematopoietic progenitors. *Cell* **109**, 29-37.

Lanz, T. A., Hosley, J. D., Adams, W. J. and Merchant, K. M. (2004). Studies of Aβ Pharmacodynamics in the Brain, Cerebrospinal Fluid, and Plasma in Young (Plaque-Free) Tg2576 Mice Using the γ-Secretase Inhibitor N2-[(2S)-2-(3,5-Difluorophenyl)-2-

hydroxyethanoyl]-N1-[(7S)-5-methyl-6-oxo-6,7-dihydro-5H-dibenzo[b,d]azepin-7-yl]-L-alaninamide (LY-411575). *J. Pharmacol. Exp. Ther.* **309**, 49-55.

Li, M., Pevny, L., Lovell-Badge, R. and Smith, A. (1998). Generation of purified neural precursors from embryonic stem cells by lineage selection. *Curr. Biol.* **8**, 971-974.

Liu, Z., Dearman, J. A., Cox, B. C., Walters, B. J., Zhang, L., Ayrault, O., Zindy, F., Gan, L., Roussel, M. F. and Zuo, J. (2012). Age-dependent in vivo conversion of mouse cochlear pillar and Deiters' cells to immature hair cells by Atoh1 ectopic expression. *J. Neurosci.* **32**, 6600-6610.

Malgrange, B., Belachew, S., Thiry, M., Nguyen, L., Rogister, B., Alvarez, M. L., Rigo, J. M., Van De Water, T. R., Moonen, G. and Lefebvre, P. P. (2002). Proliferative generation of mammalian auditory hair cells in culture. *Mech. Dev.* **112**, 79-88.

Maricich, S. M., Wellnitz, S. A., Nelson, A. M., Lesniak, D. R., Gerling, G. J., Lumpkin, E. A. and Zoghbi, H. Y. (2009). Merkel cells are essential for light-touch responses. *Science* **324**, 1580-1582.

Marro, S., Pang, Z. P., Yang, N., Tsai, M. C., Qu, K., Chang, H. Y., Sudhof, T. C. and Wernig, M. (2011). Direct lineage conversion of terminally differentiated hepatocytes to functional neurons. *Cell stem cell* **9**, 374-382.

Matei, V., Pauley, S., Kaing, S., Rowitch, D., Beisel, K. W., Morris, K., Feng, F., Jones, K., Lee, J. and Fritzsch, B. (2005). Smaller inner ear sensory epithelia in Neurog 1 null mice are related to earlier hair cell cycle exit. *Dev. Dyn.* **234**, 633- 650.

Mulvaney, J. and Dabdoub, A. (2012). Atoh1, an essential transcription factor in neurogenesis and intestinal and inner ear development: function, regulation, and context dependency. *J. Assoc. Res. Otolaryngol.* **13**, 281-293.

Newton, F. G., zur Lage, P. I., Karak, S., Moore, D. J., Gopfert, M. C. and Jarman, A. P. (2012). Forkhead transcription factor Fd3F cooperates with Rfx to regulate a gene expression program for mechanosensory cilia specialization. *Dev. Cell* **22**, 1221-1233.

Ninkina, N. N., Stevens, G. E., Wood, J. N. and Richardson, W. D. (1993). A novel Brn3-like POU transcription factor expressed in subsets of rat sensory and spinal cord neurons. *Nucleic Acids Res.* **21**, 3175-3182.

Oshima, K., Shin, K., Diensthuber, M., Peng, A. W., Ricci, A. J. and Heller, S. (2010). Mechanosensitive hair cell-like cells from embryonic and induced pluripotent stem cells. *Cell* **141**, 704-716.

Pan, N., Jahan, I., Kersigo, J., Duncan, J. S., Kopecky, B. and Fritzsch, B. (2012). A novel Atoh1 "self-terminating" mouse model reveals the necessity of proper Atoh1 level and duration for hair cell differentiation and viability. *PloS one* **7**, e30358.

Represa, J., Sanchez, A., Miner, C., Lewis, J. and Giraldez, F. (1990). Retinoic Acid Modulation of the Early Development of the Inner-Ear Is Associated with the Control of C-Fos Expression. *Development* **110**, 1081-1090.

Rose, M. F., Ren, J., Ahmad, K. A., Chao, H. T., Klisch, T. J., Flora, A., Greer, J. J. and Zoghbi, H. Y. (2009). Math1 Is Essential for the Development of Hindbrain Neurons Critical for Perinatal Breathing. *Neuron* **64**, 341-354.

Ruben, R. J. (1967). Development of the inner ear of the mouse: a radioautographic study of terminal mitoses. *Acta Otolaryngol.* **220**, 1-44.

Sage, C., Huang, M., Vollrath, M. A., Brown, M. C., Hinds, P. W., Corey, D. P., Vetter, D. E. and Chen, Z. Y. (2006). Essential role of retinoblastoma protein in mammalian hair cell development and hearing. *Proc. Natl. Acad. Sci. USA* **103**, 7345-7350.

Sekerkova, G., Zheng, L., Loomis, P. A., Mugnaini, E. and Bartles, J. R. (2006). Espins and the actin cytoskeleton of hair cell stereocilia and sensory cell microvilli. *Cell. Mol. Life Sci.* **63**, 2329-2341.

Shroyer, N. F., Wallis, D., Venken, K. J. T., Bellen, H. J. and Zoghbi, H. Y. (2005). Gfi1 functions downstream of Math1 to control intestinal secretory cell subtype allocation and differentiation. *Genes Dev.* **19**, 2412–2417.

Siemens, J., Lillo, C., Dumont, R. A., Reynolds, A., Williams, D. S., Gillespie, P. G. and Muller, U. (2004). Cadherin 23 is a component of the tip link in hair-cell stereocilia. *Nature* **428**, 950-955.

Smyth, G. K. (2004). Linear models and empirical bayes methods for assessing differential expression in microarray experiments. *Stat. Appl. Genet. Mol. Biol.* **3**, 1544-6115.

Stubbs, J. L., Oishi, I., Izpisua Belmonte, J. C. and Kintner, C. (2008). The forkhead protein Foxj1 specifies node-like cilia in Xenopus and zebrafish embryos. *Nat. Genet.* **40**, 1454-1460.

Szymczak, A. L., Workman, C. J., Wang, Y., Vignali, K. M., Dilioglou, S., Vanin, E. F. and Vignali, D. A. A. (2004). Correction of multi-gene deficiency in vivo using a single 'self-cleaving' 2A peptide–based retroviral vector. *Nat. Biotechnol.* **22**, 589-594.

Takahashi, Y., Watanabe, T., Nakagawa, S., Kawakami, K. and Sato, Y. (2008). Transposon-mediated stable integration and tetracycline-inducible expression of electroporated transgenes in chicken embryos. *Methods Cell Biol.* **87**, 271-280.

Ting, D. T., Kyba, M. and Daley, G. Q. (2005). Inducible transgene expression in mouse stem cells. *Methods Mol. Med.* **105**, 23-46.

Tsuda, H., Jafar-Nejad, H., Patel, A. J., Sun, Y., Chen, H. K., Rose, M. F., Venken, K. J. T., Botas, J., Orr, H. T., Bellen, H. J. et al. (2005). The AXH domain of Ataxin-1 mediates neurodegeneration through its interaction with Gfi-1/senseless proteins. *Cell* **122**, 633-644.

Vierbuchen, T., Ostermeier, A., Pang, Z. P., Kokubu, Y., Sudhof, T. C. and Wernig, M. (2010). Direct conversion of fibroblasts to functional neurons by defined factors. *Nature* **463**, 1035-1041.

Wallis, D., Hamblen, M., Zhou, Y., Venken, K. J. T., Schumacher, A., Grimes, H. L., Zoghbi, H. Y., Orkin, S. H. and Bellen, H. J. (2003). The zinc finger transcription factor Gfi1, implicated in lymphomagenesis, is required for inner ear hair cell differentiation and survival. *Development* **130**, 221-232.

Wang, S. W., Mu, X., Bowers, W. J., Kim, D. S., Plas, D. J., Crair, M. C., Federoff, H. J., Gan, L. and Klein, W. H. (2002). Brn3b/Brn3c double knockout mice reveal an unsuspected role for Brn3c in retinal ganglion cell axon outgrowth. *Development* **129**, 467-477.

Warchol, M. E. (2011). Sensory regeneration in the vertebrate inner ear: differences at the levels of cells and species. *Hear. Res.* **273**, 72-79.

Woods, C., Montcouquiol, M. and Kelley, M. W. (2004). Math1 regulates development of the sensory epithelium in the mammalian cochlea. *Nat. Neurosci.* **7**, 1310-1318.

Xiang, M., Gao, W.-Q., Hasson, T. and Shin, J. J. (1998). Requirement for Brn-3c in maturation and survival, but not in fate determination of inner ear hair cells. *Development* **125**, 3935-3946.

Xiang, M., Zhou, L., Macke, J. P., Yoshioka, T., Hendry, S. H., Eddy, R. L., Shows, T. B. and Nathans, J. (1995). The Brn-3 family of POU-domain factors: primary structure, binding specificity, and expression in subsets of retinal ganglion cells and somatosensory neurons. *J. Neurosci.* **15**, 4762-4785.

Xiang, M., Gan, L., Li, D., Chen, Z. Y., Zhou, L., O'Malley, B. W., Jr., Klein, W. and Nathans, J. (1997). Essential role of POU-domain factor Brn-3c in auditory and vestibular hair cell development. *Proc. Natl. Acad. Sci. USA* **94**, 9445-9450.

Yang, Q., Bermingham, N. A., Finegold, M. J. and Zoghbi, H. Y. (2001). Requirement of Math1 for secretory cell lineage commitment in the mouse intestine. *Science* **294**, 2155-2158.

Zheng, J. L. and Gao, W. Q. (2000). Overexpression of Math1 induces robust production of extra hair cells in postnatal rat inner ears. *Nat. Neurosci.* **3**, 580-586.

Zheng, J. L., Shou, J. Y., Guillemot, F., Kageyama, R. and Gao, W. Q. (2000). Hes1 is a negative regulator of inner ear hair cell differentiation. *Development* **127**, 4551-4560.

Zheng, L. L., Sekerkova, G., Vranich, K., Tilney, L. G., Mugnaini, E. and Bartles, J. R. (2000). The deaf jerker mouse has a mutation in the gene encoding the espin actin-bundling proteins of hair cell stereocilia and lacks espins. *Cell* **102**, 377-385.

A

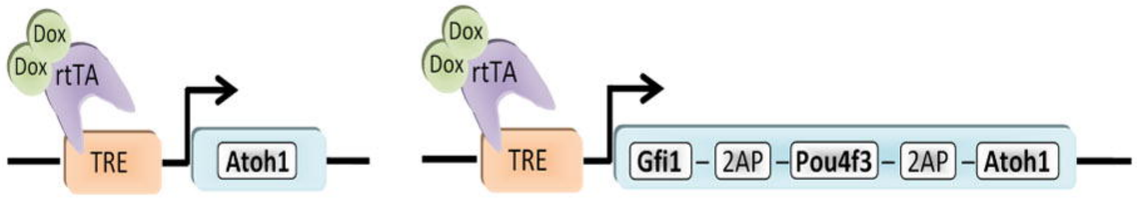
Dox
Dox
rtTA
TRE
Atoh1
Dox
Dox
rtTA
TRE
Gfi1
2AP
Pou4f3
2AP
Atoh1

B

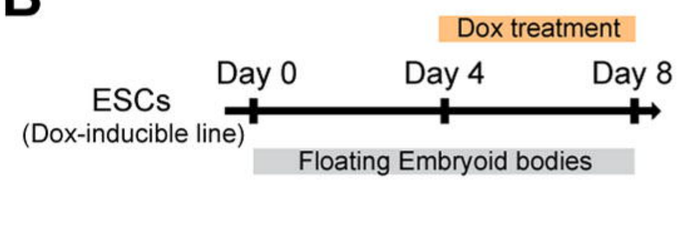
Dox treatment
Day 0
Day 4
Day 8
ESCs
(Dox-inducible line)
Floating Embryoid bodies

C

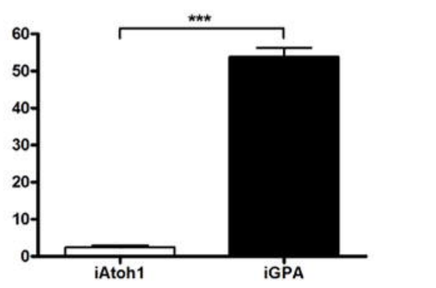
% Myo7a+ cells relative to induced cells (Atoh1+ cells)
***
60
50
40
30
20
10
0
iAtoh1
iGPA

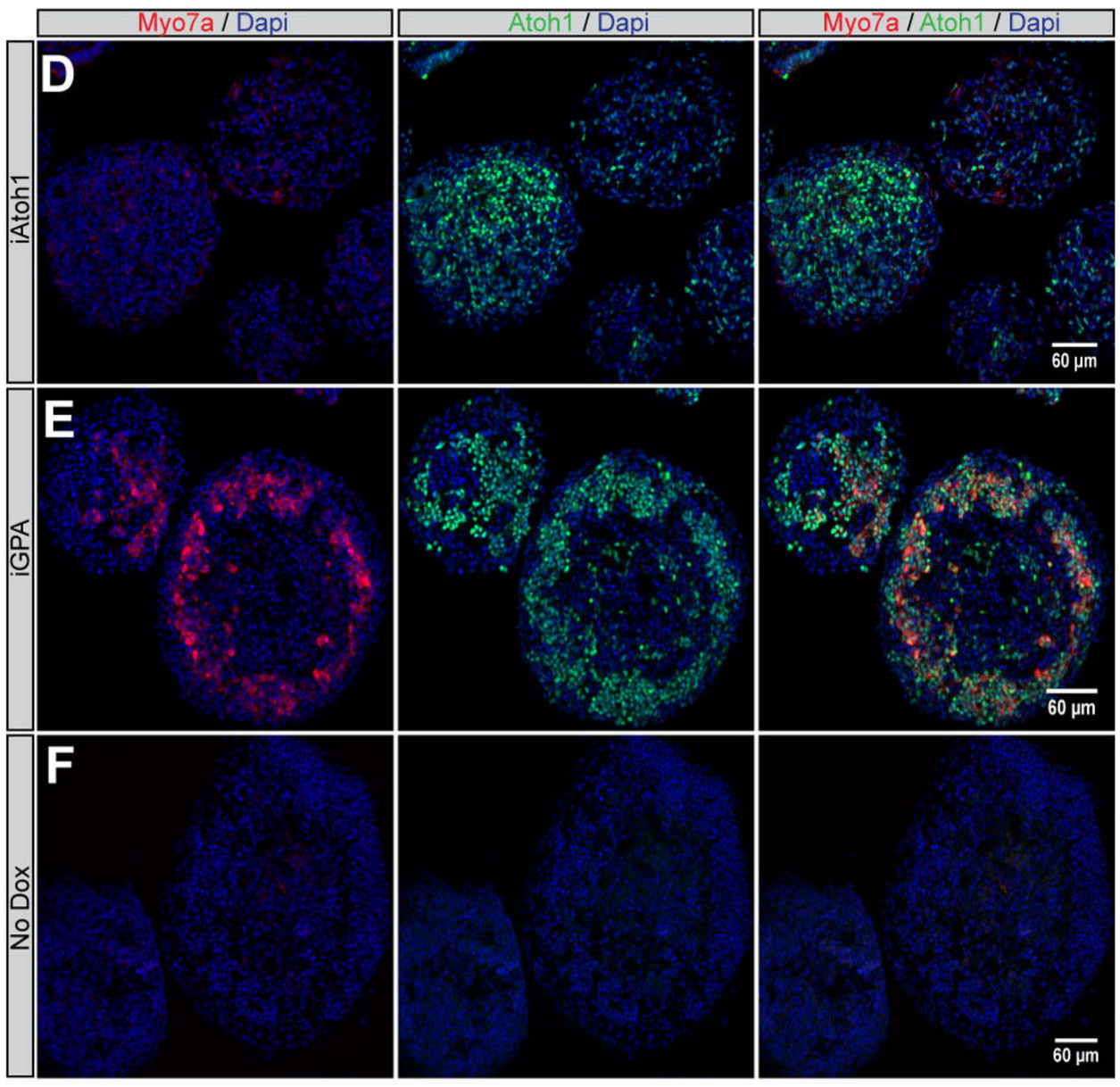
Myo7a / Dapi
Atoh1 / Dapi
Myo7a / Atoh1 / Dapi
iAtoh1
D
E
F
iGPA
No Dox
60 µm

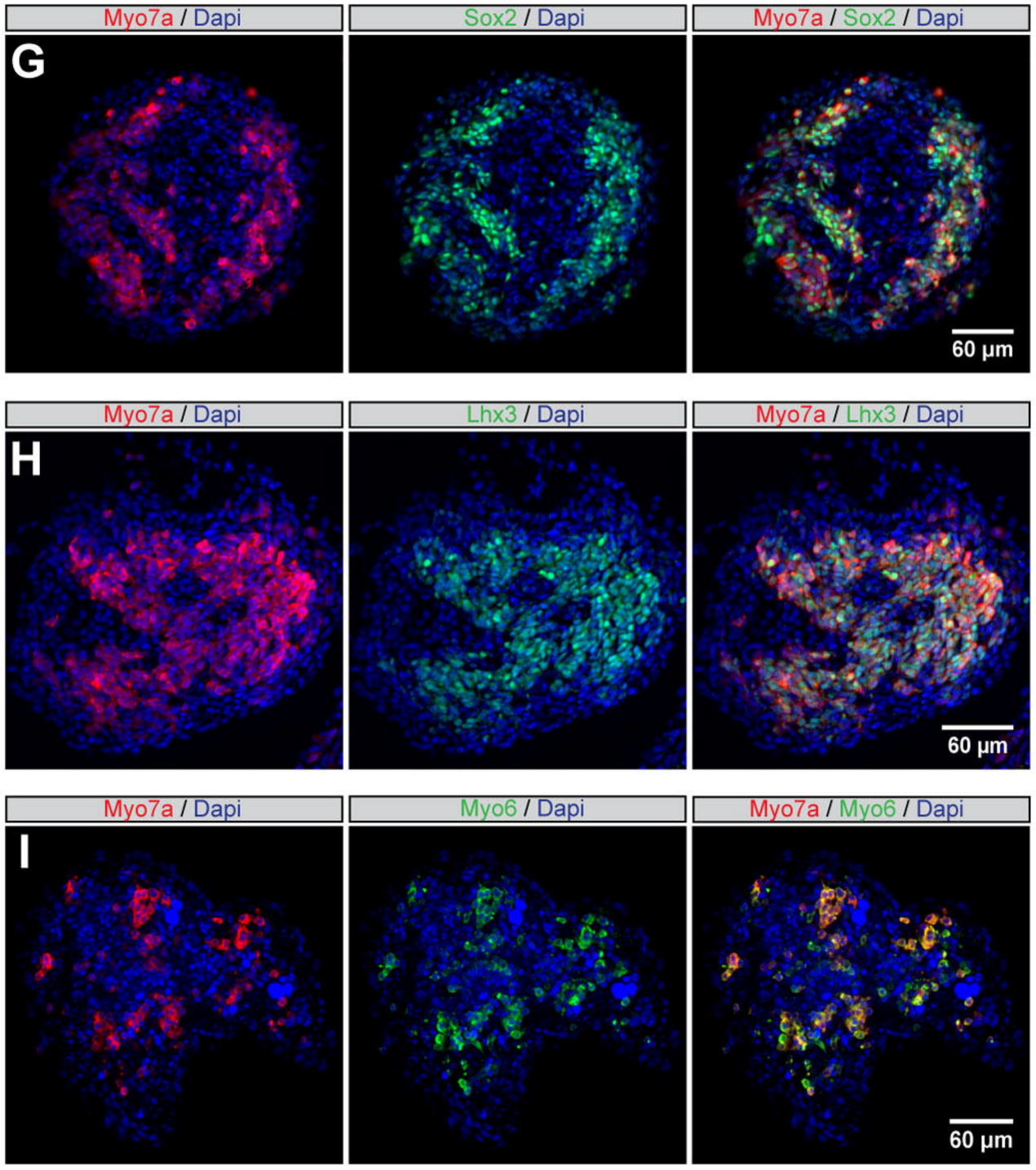
Myo7a / Dapi
Sox2 / Dapi
Myo7a / Sox2 / Dapi
G
Lhx3 / Dapi
Myo7a / Lhx3 / Dapi
H
Myo6 / Dapi
Myo7a / Myo6 / Dapi
I
60 µm

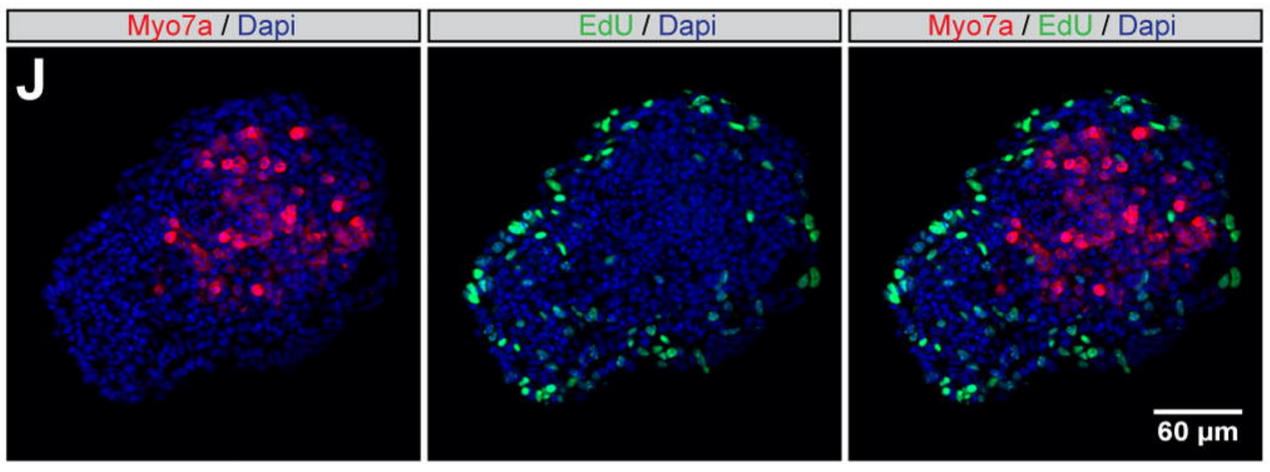
Myo7a / Dapi
EdU / Dapi
Myo7a / EdU / Dapi
J
60 µm

K

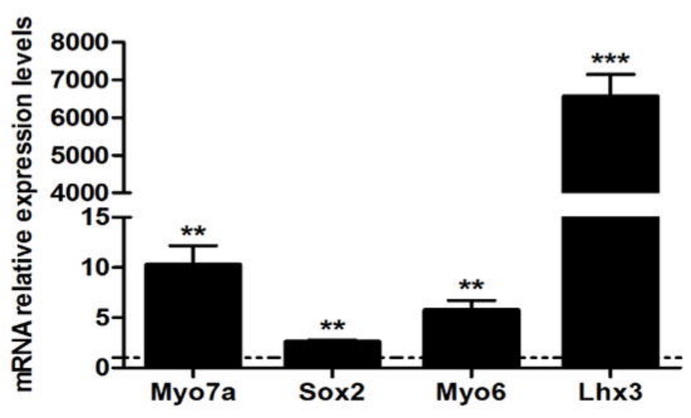
mRNA relative expression levels
8000
7000
6000
5000
4000
15
10
5
0
**
**
**
***
Myo7a
Sox2
Myo6
Lhx3

A

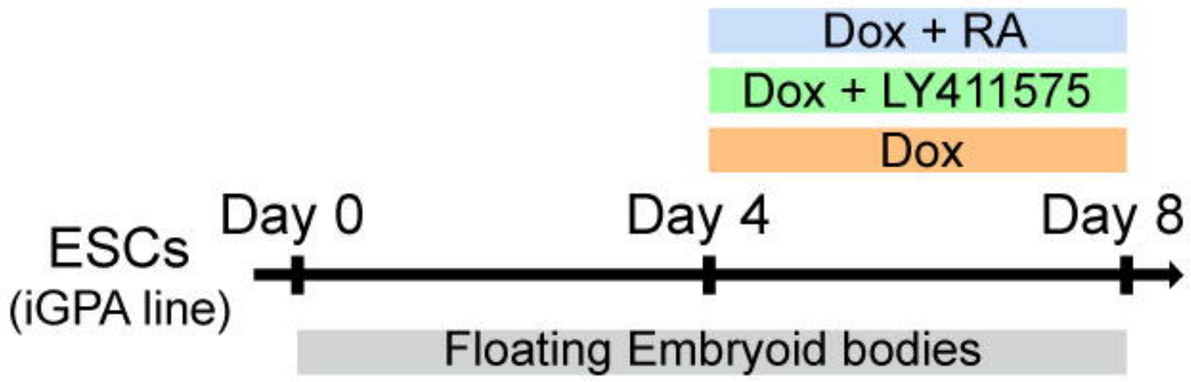
Dox + RA
Dox + LY411575
Dox
Day 0
Day 4
Day 8
ESCs
(iGPA line)
Floating Embryoid bodies

B

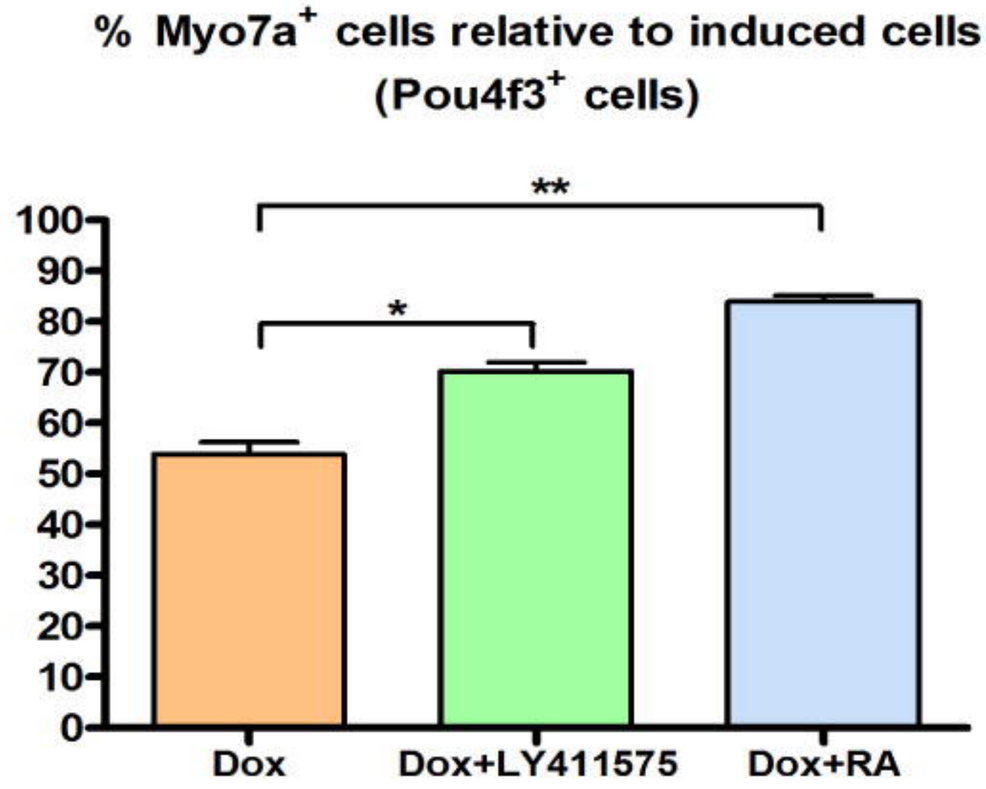
% Myo7a+ cells relative to induced cells
(Pou4f3+ cells)
100
90
80
70
60
50
40
30
20
10
0
**
*
Dox
Dox+LY411575
Dox+RA

C

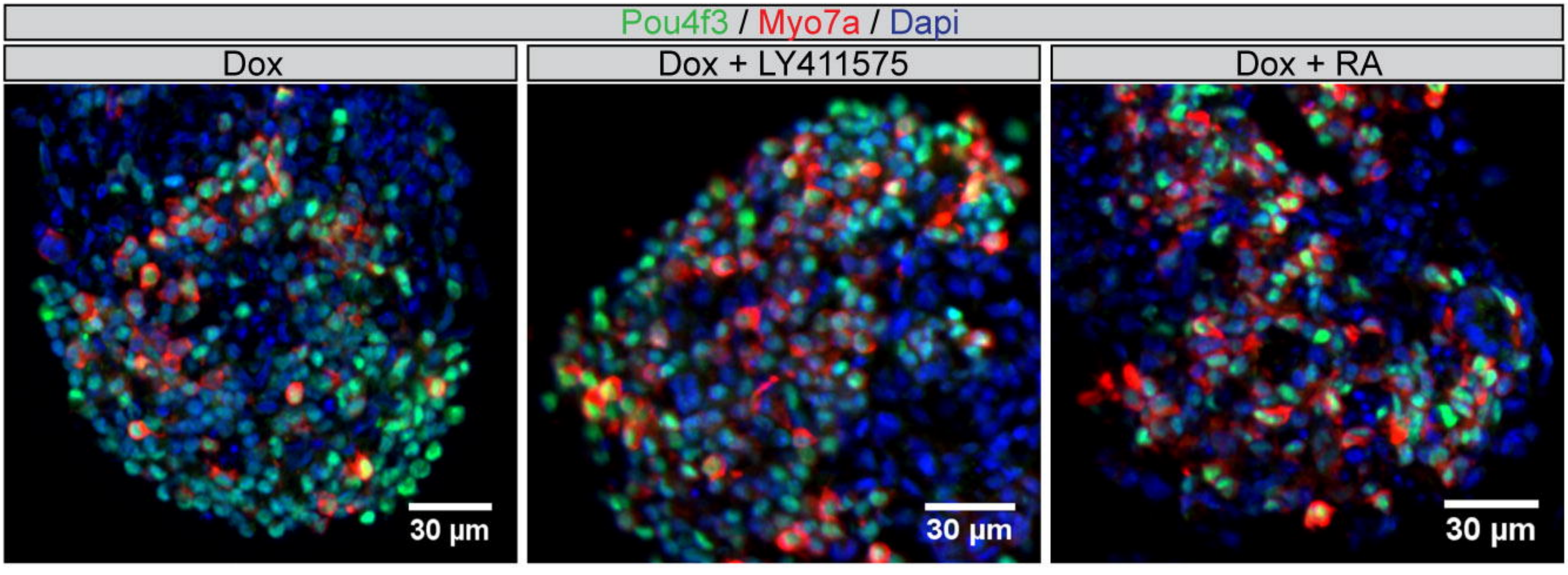
Pou4f3 / Myo7a / Dapi
Dox
Dox + LY411575
Dox + RA
30 µm
30 µm
30 µm

D

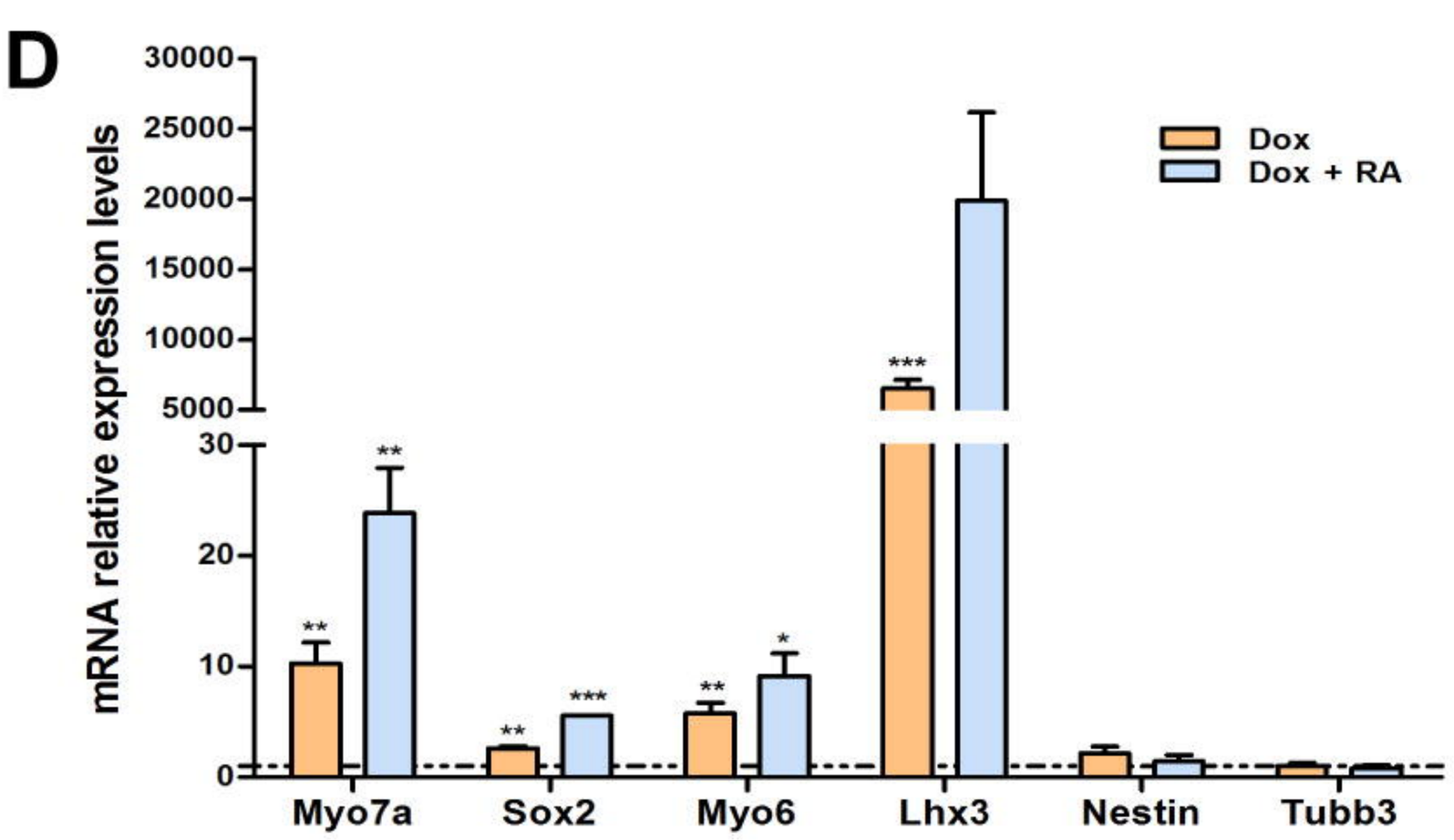
mRNA relative expression levels
30000
25000
20000
15000
10000
5000
30
20
10
0
Dox
Dox + RA
Myo7a
Sox2
Myo6
Lhx3
Nestin
Tubb3

A

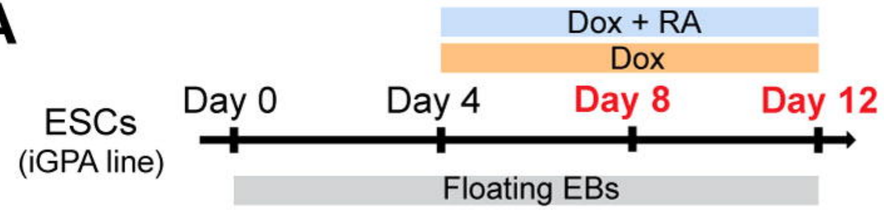
Dox + RA
Dox
ESCs
(iGPA line)
Day 0
Day 4
Day 8
Day 12
Floating EBs

E

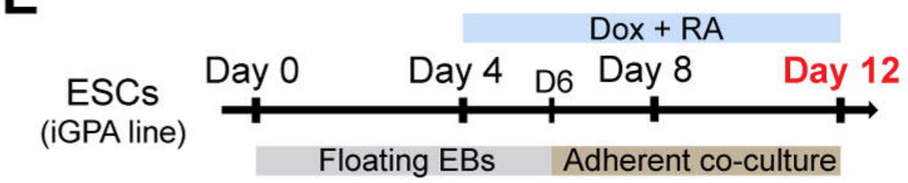
Dox + RA
ESCs
(iGPA line)
Day 0
Day 4
D6
Day 8
Day 12
Floating EBs
Adherent co-culture

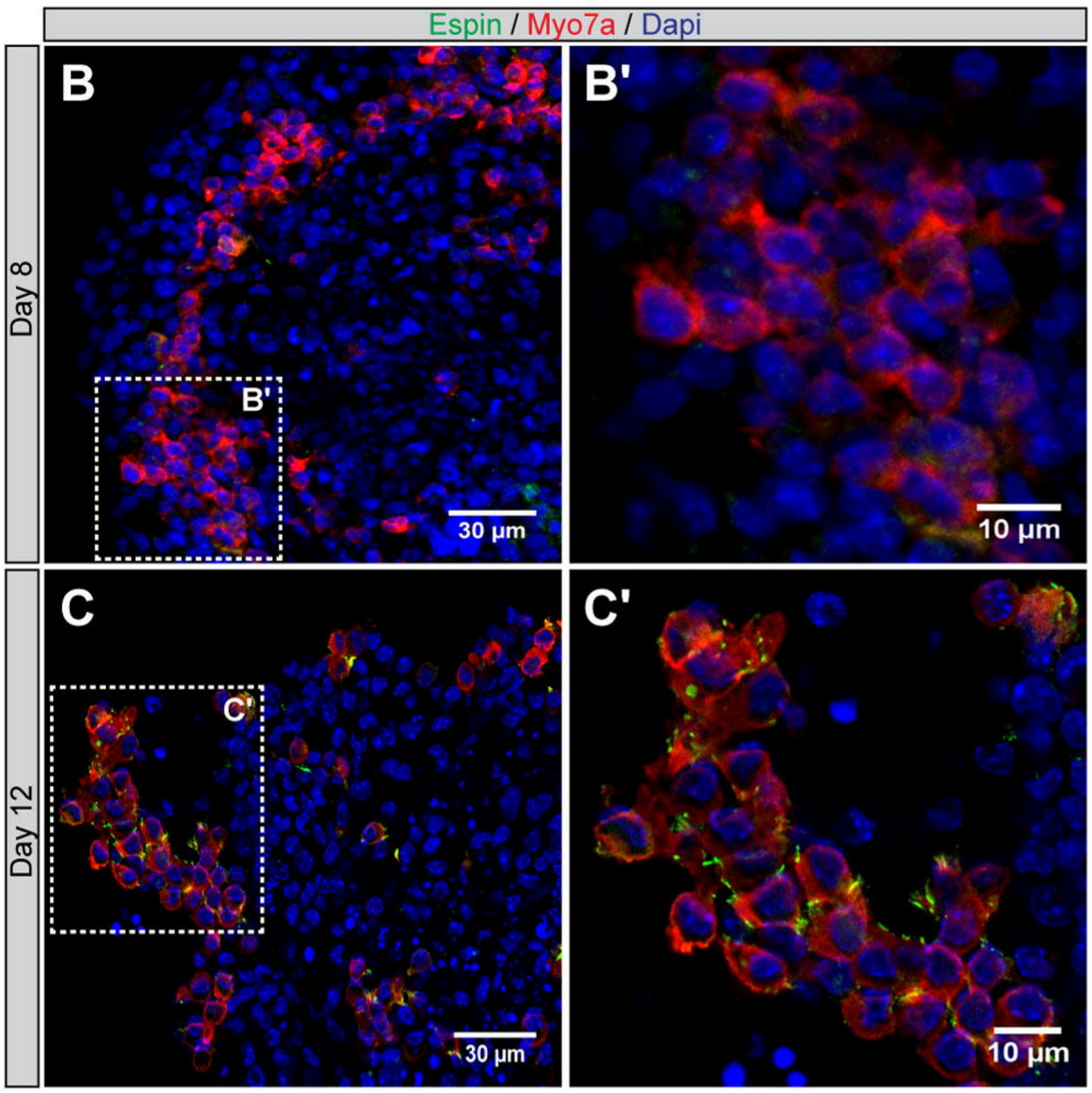
Espin / Myo7a / Dapi
Day 8
Day 12
B
B'
C
C'
30 µm
10 µm

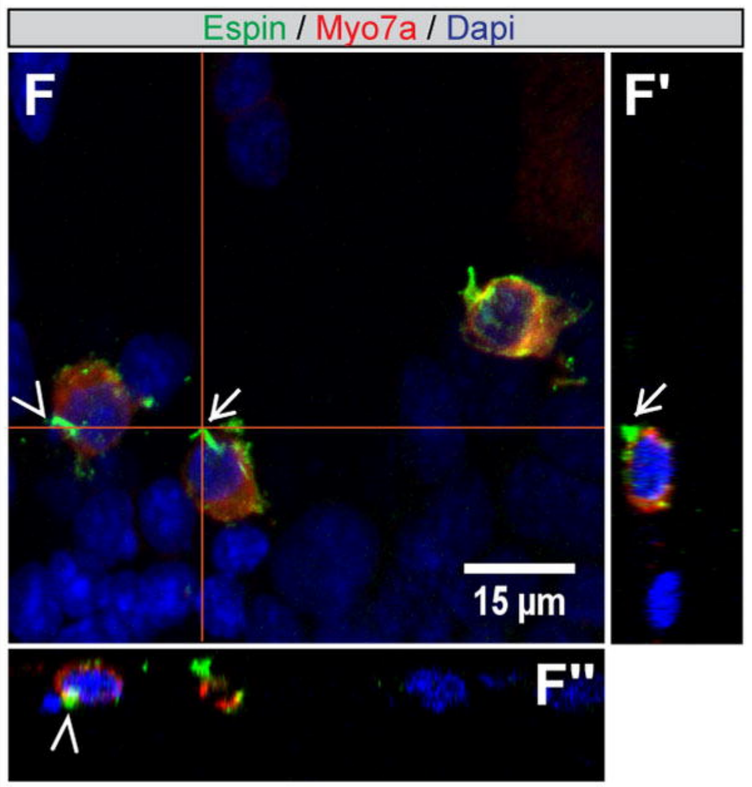
Espin / Myo7a / Dapi
F
F'
F''
15 µm

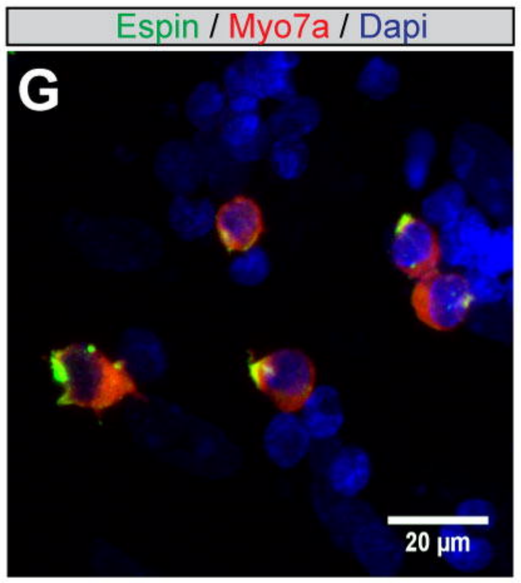
Espin / Myo7a / Dapi
G
20 µm

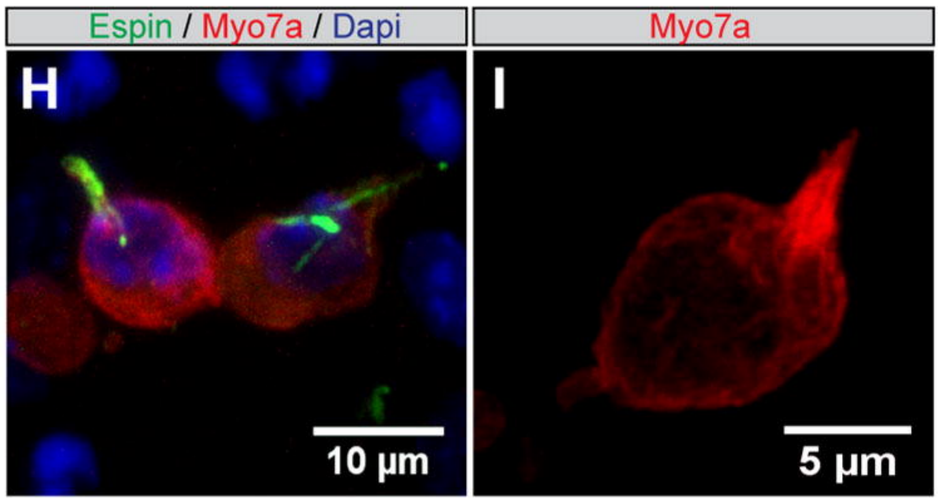
Espin / Myo7a / Dapi
Myo7a
H
I
10 µm
5 µm

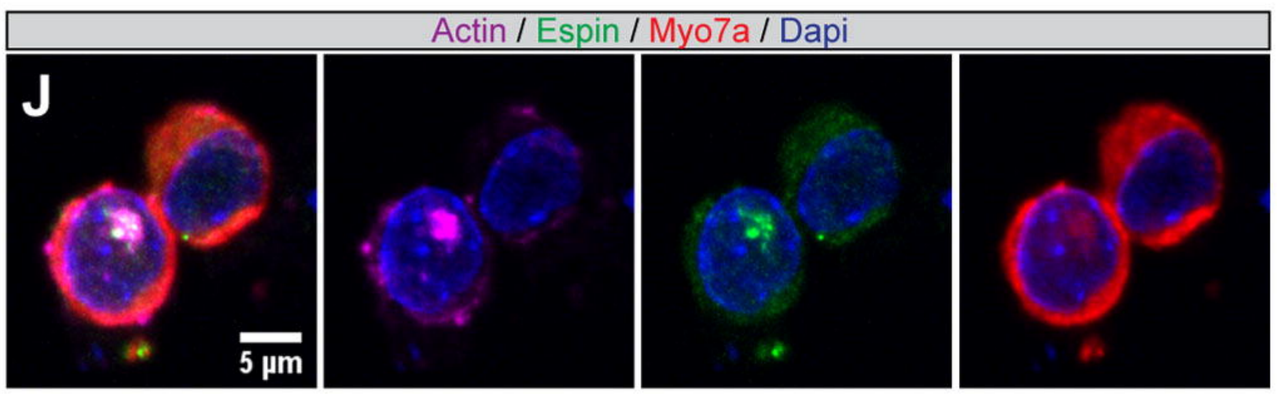
Actin / Espin / Myo7a / Dapi
J
5 µm

D

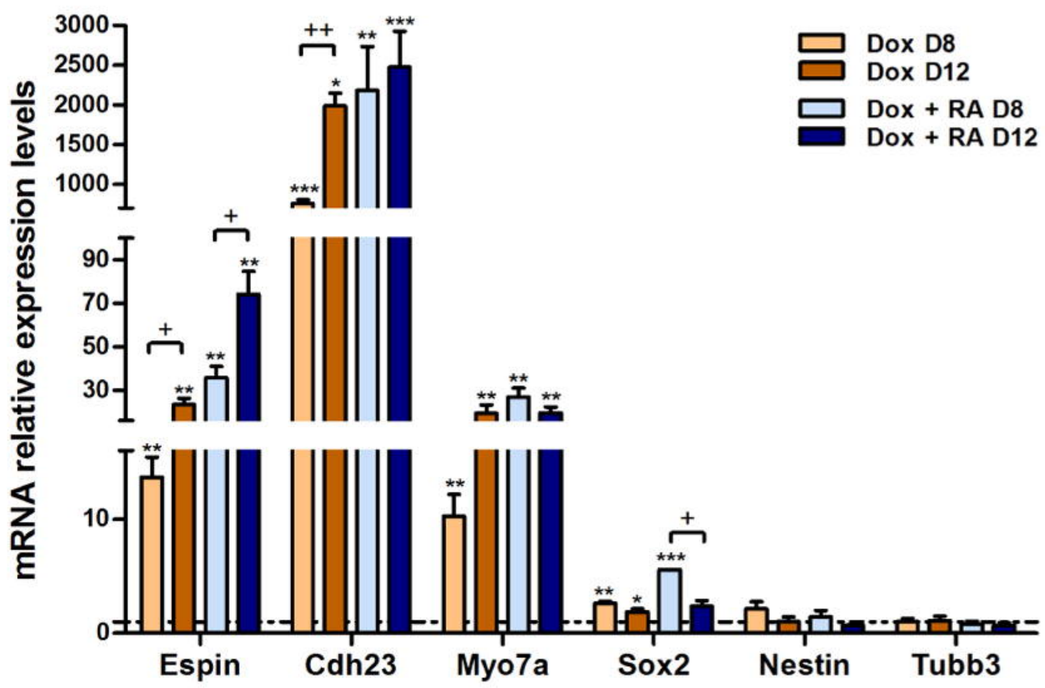
mRNA relative expression levels
Dox D8
Dox D12
Dox + RA D8
Dox + RA D12
Espin
Cdh23
Myo7a
Sox2
Nestin
Tubb3

K

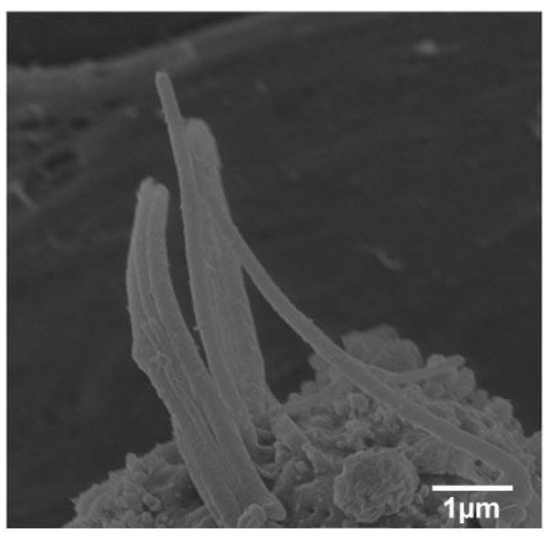
1µm

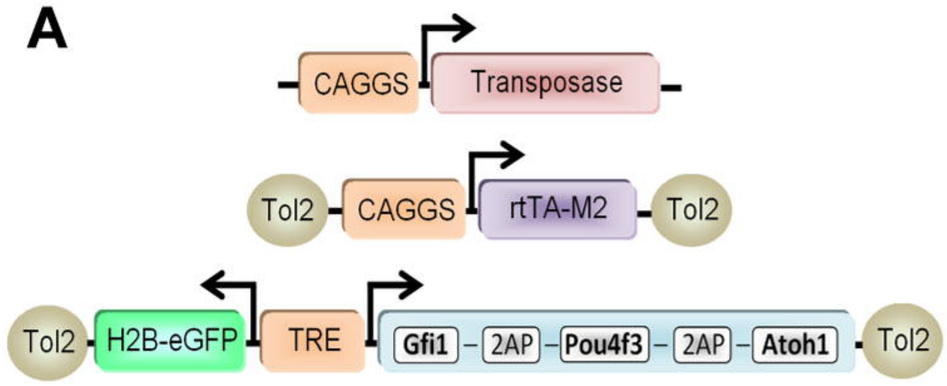
A
CAGGS
Transposase
Tol2
CAGGS
rtTA-M2
Tol2
Tol2
H2B-eGFP
TRE
Gfi1
2AP
Pou4f3
2AP
Atoh1
Tol2

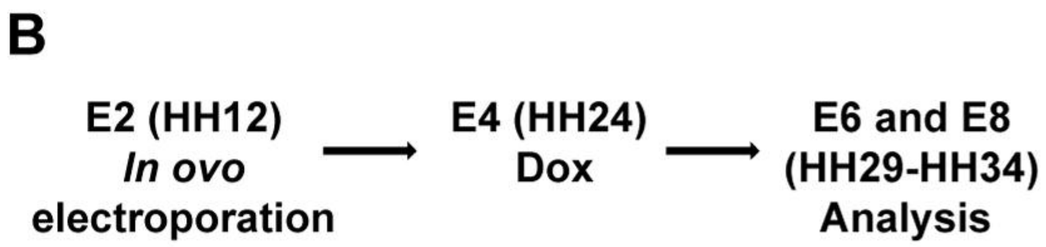
B
E2 (HH12)
In ovo
electroporation
E4 (HH24)
Dox
E6 and E8
(HH29-HH34)
Analysis

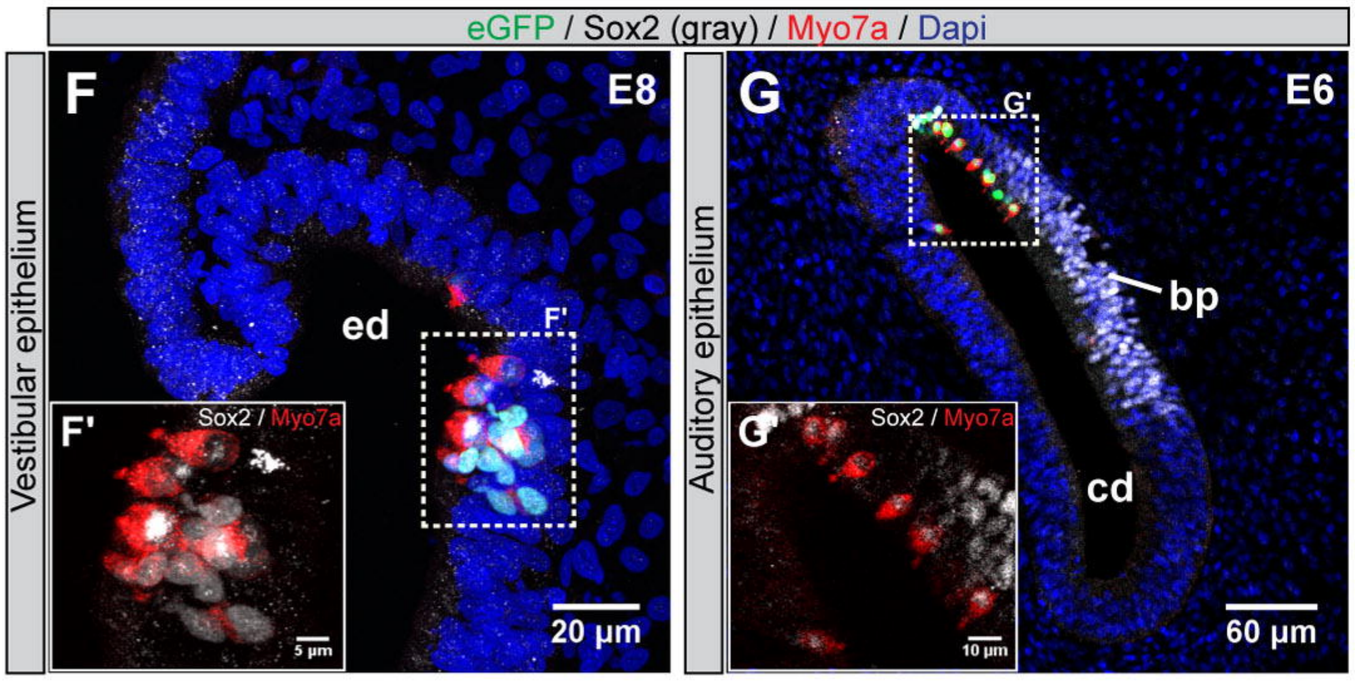
eGFP / Sox2 (gray) / Myo7a / Dapi
F
E8
ed
F'
Sox2 / Myo7a
5 µm
20 µm
Vestibular epithelium
G
E6
G'
bp
cd
Sox2 / Myo7a
10 µm
60 µm
Auditory epithelium

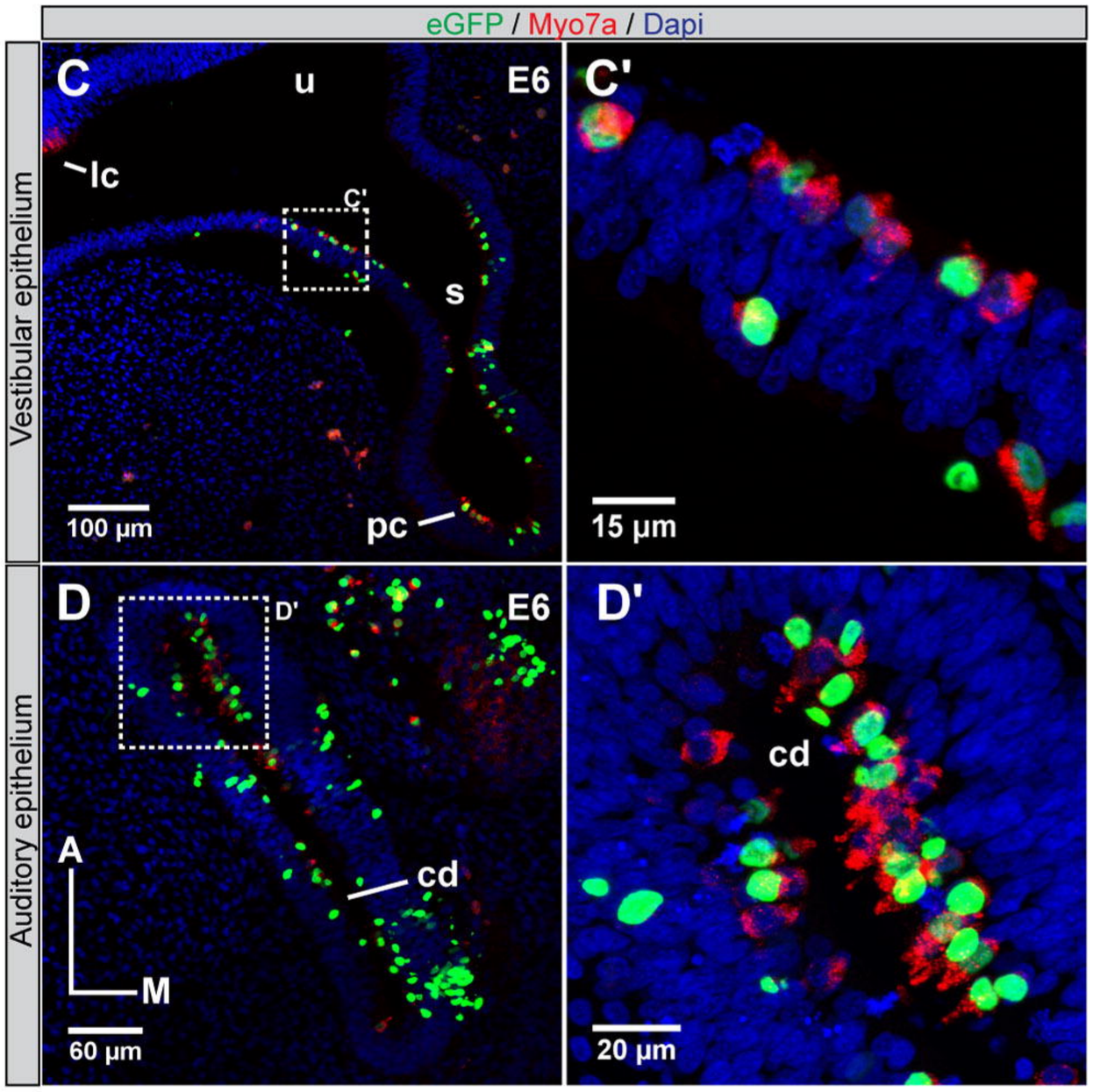
eGFP / Myo7a / Dapi
C
u
E6
lc
C'
s
100 µm
pc
15 µm
Vestibular epithelium
D
D'
E6
cd
A
M
60 µm
20 µm
Auditory epithelium

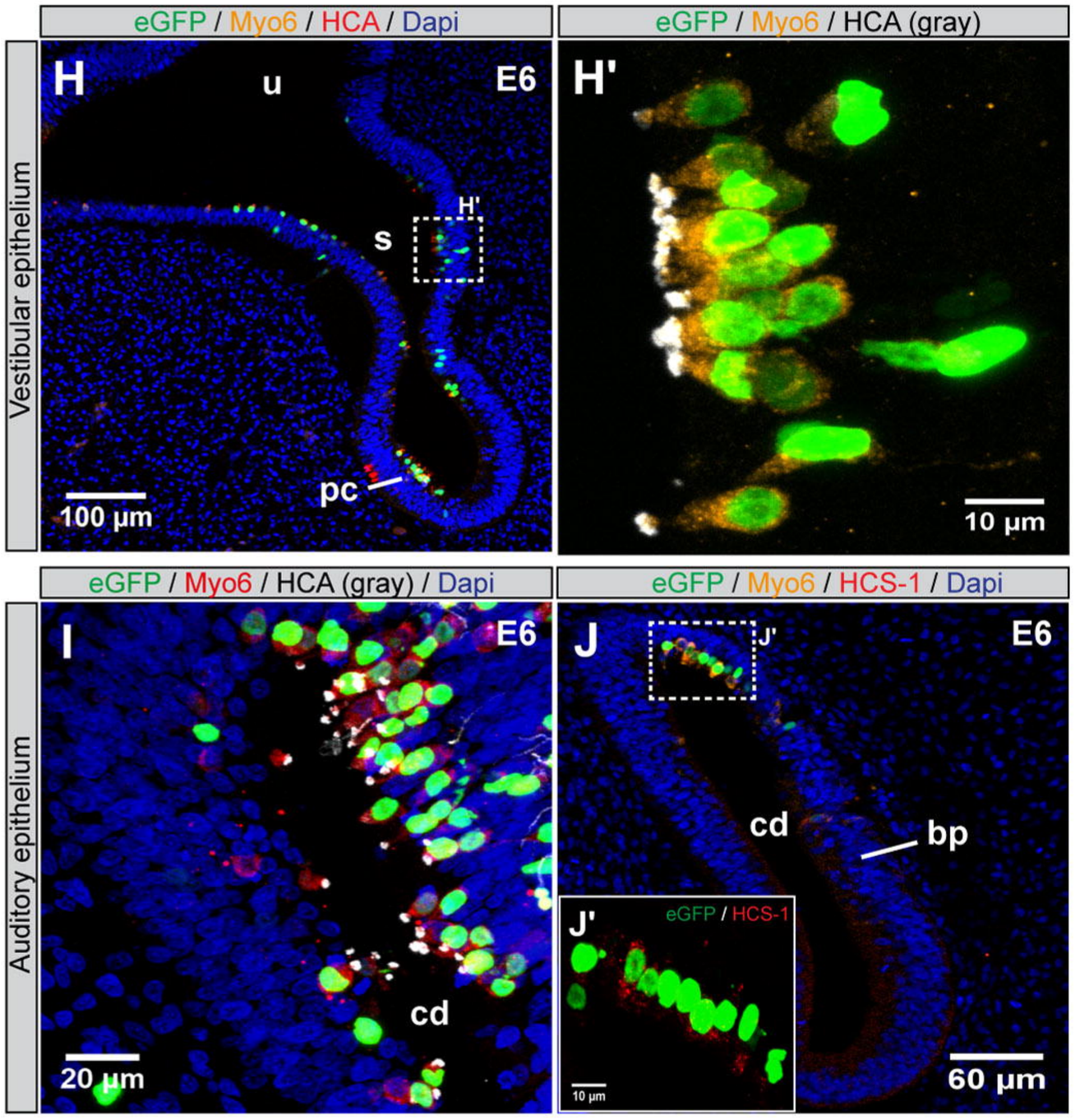
eGFP / Myo6 / HCA / Dapi
H
u
E6
H'
s
pc
100 µm
Vestibular epithelium
eGFP / Myo6 / HCA (gray)
H'
10 µm
eGFP / Myo6 / HCA (gray) / Dapi
I
E6
cd
20 µm
Auditory epithelium
eGFP / Myo6 / HCS-1 / Dapi
J
J'
E6
cd
bp
J'
eGFP / HCS-1
10 µm
60 µm

eGFP / Myo6 / Dapi
E
E6
mu
ms
*
lc
E'
80 µm
E'
10 µm
eGFP / Myo6

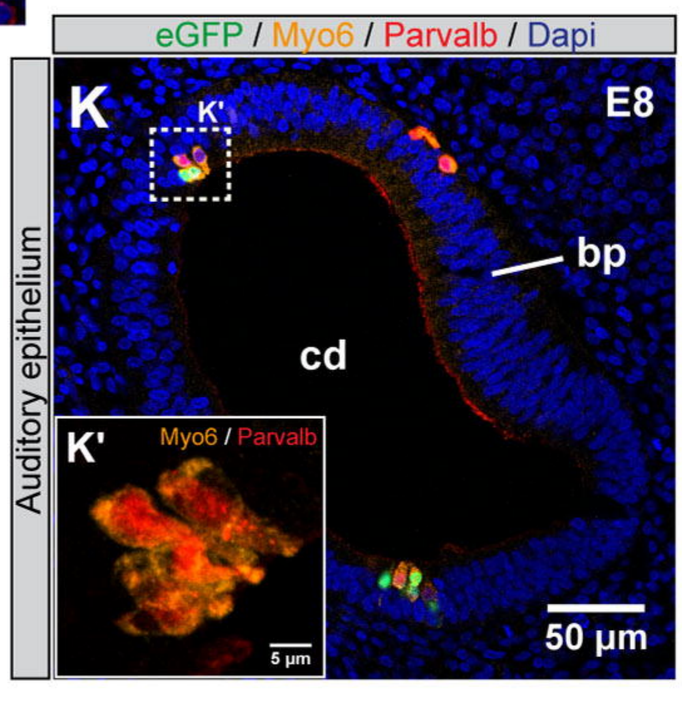
eGFP / Myo6 / Parvalb / Dapi
K
K'
E8
bp
cd
K'
Myo6 / Parvalb
5 µm
50 µm
Auditory epithelium

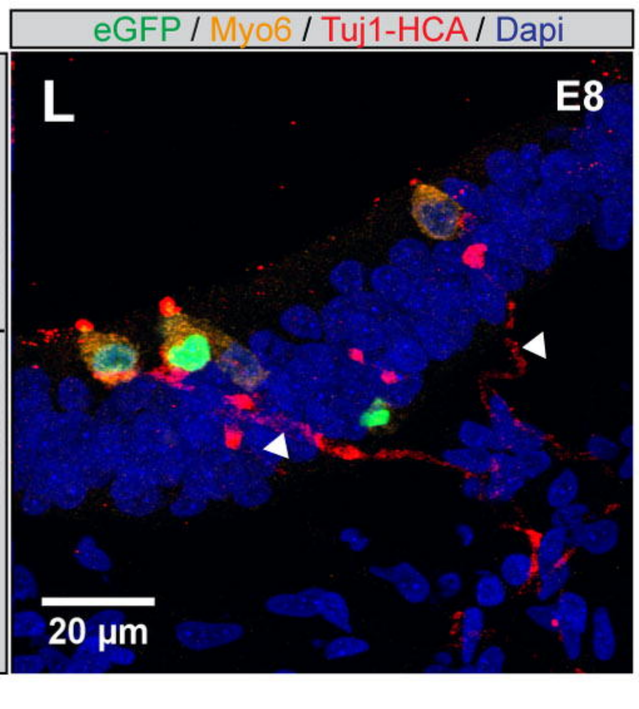
eGFP / Myo6 / Tuj1-HCA / Dapi
L
E8
20 µm
Vestibular epithelium

A

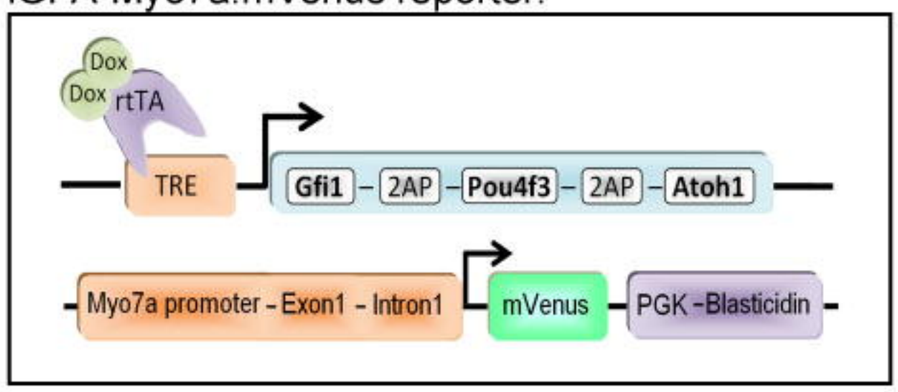
iGPA-Myo7a:mVenus reporter:
Dox
Dox
rtTA
TRE
Gfi1
2AP
Pou4f3
2AP
Atoh1
Myo7a promoter - Exon1 - Intron1
mVenus
PGK -Blasticidin

B

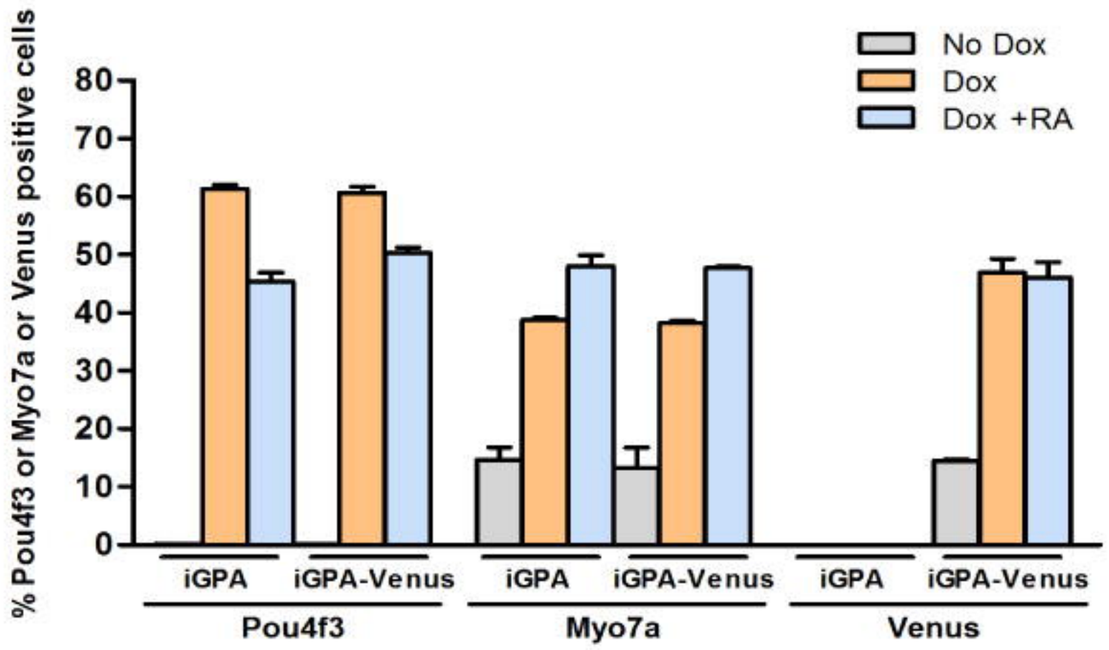
% Pou4f3 or Myo7a or Venus positive cells
No Dox
Dox
Dox +RA
iGPA
iGPA-Venus
Pou4f3
Myo7a
Venus

C

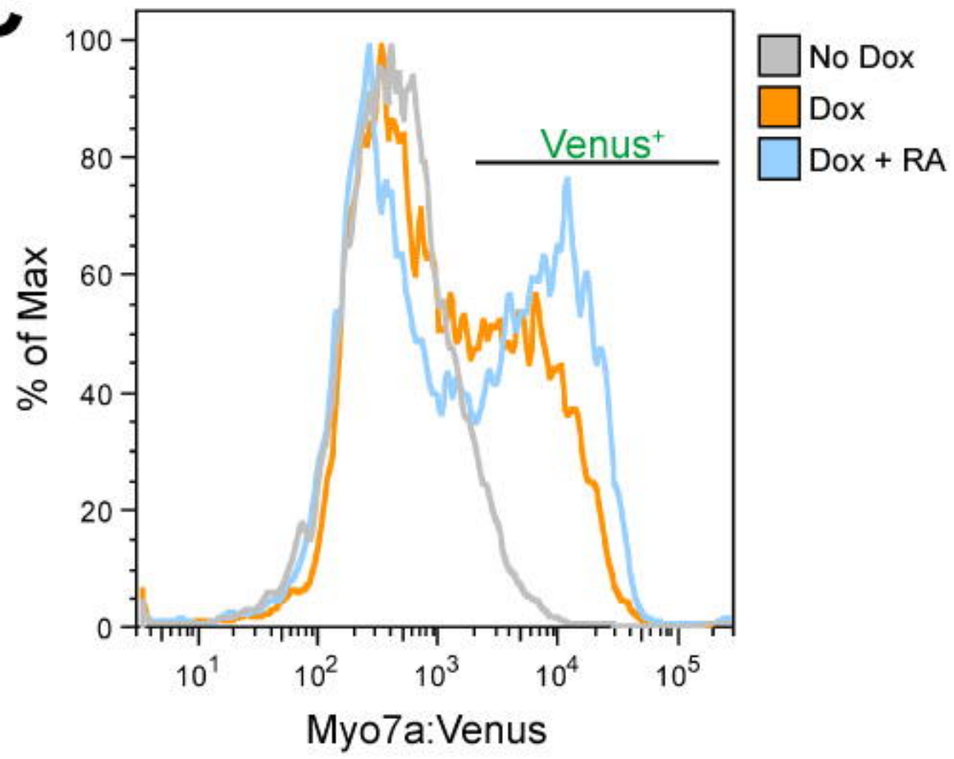
Venus+
No Dox
Dox
Dox + RA
% of Max
Myo7a:Venus

D

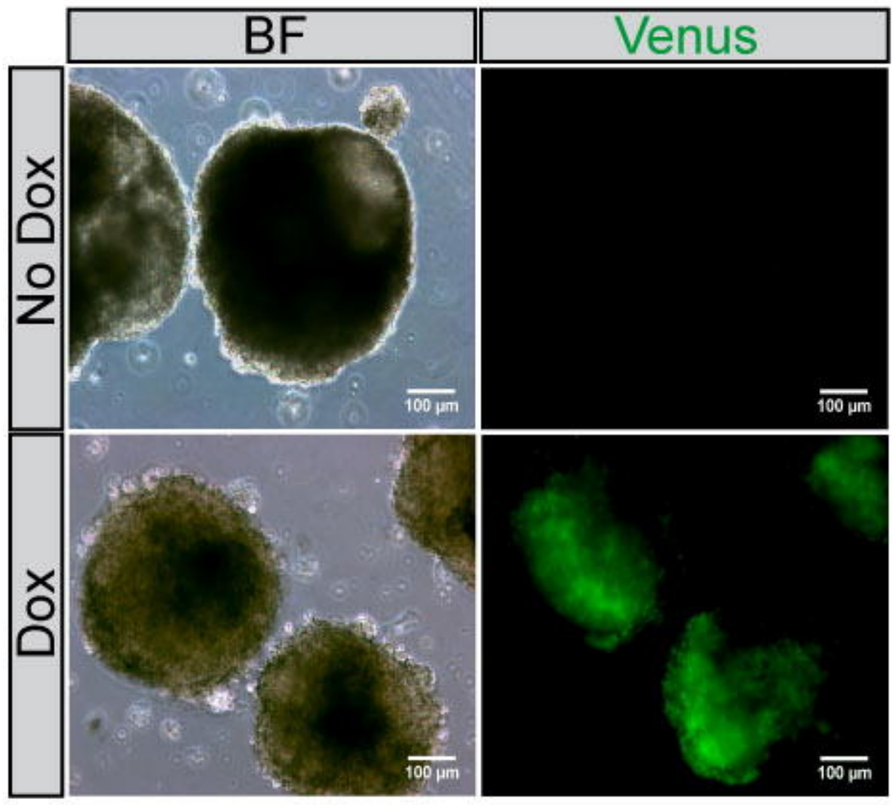
BF
Venus
No Dox
Dox
100 µm

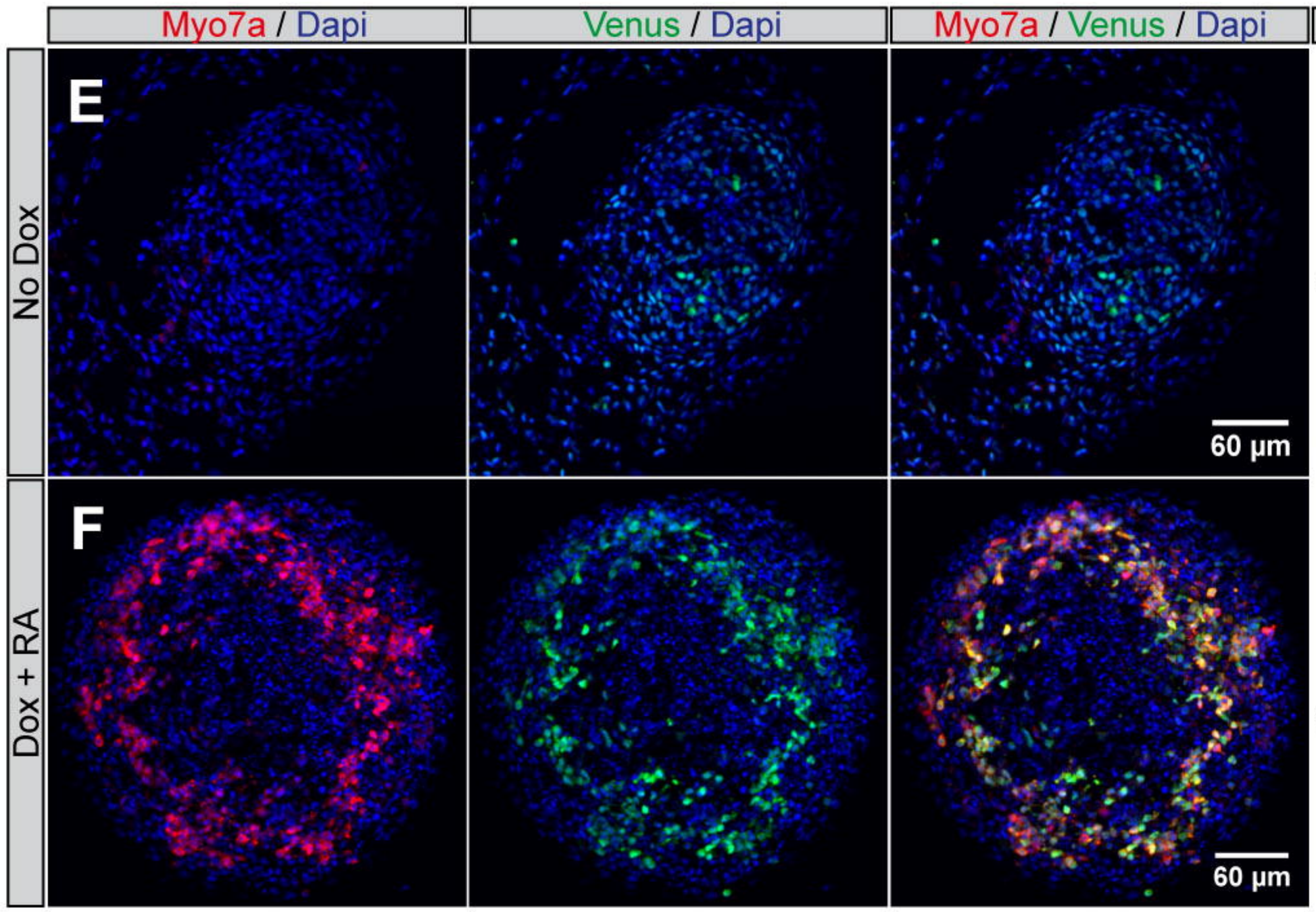
Myo7a / Dapi
Venus / Dapi
Myo7a / Venus / Dapi
FC-IS
E
F
No Dox
Dox + RA
60 µm
12%
3%
72%
13%
38%
36%
14%
R=0,601
Venus
Myo7a

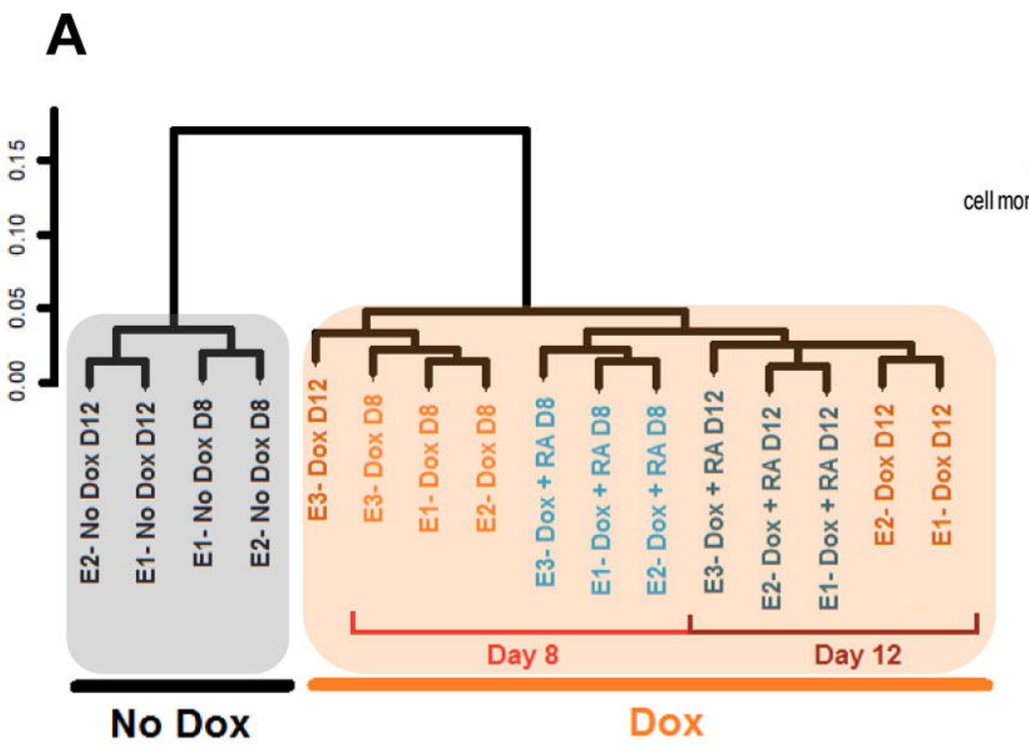
A
0.15
0.10
0.05
0.00
E2- No Dox D12
E1- No Dox D12
E1- No Dox D8
E2- No Dox D8
E3- Dox D12
E3- Dox D8
E1- Dox D8
E2- Dox D8
E3- Dox + RA D8
E1- Dox + RA D8
E2- Dox + RA D8
E3- Dox + RA D12
E2- Dox + RA D12
E1- Dox + RA D12
E2- Dox D12
E1- Dox D12
Day 8
Day 12
No Dox
Dox

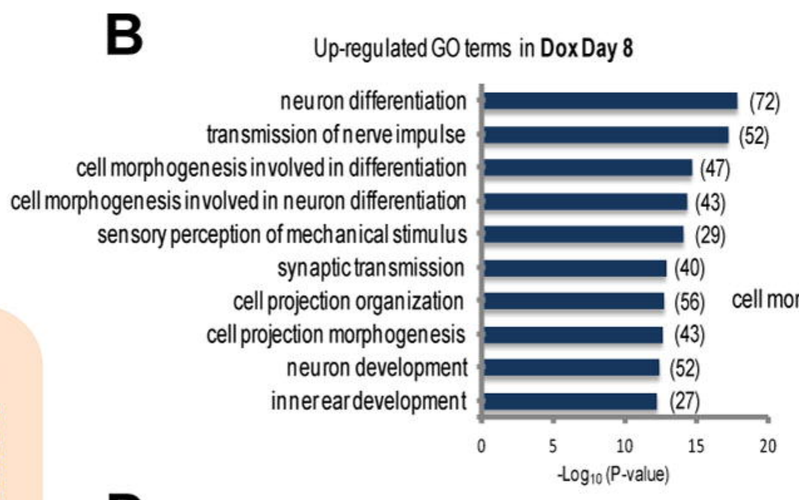
B
Up-regulated GO terms in Dox Day 8
neuron differentiation (72)
transmission of nerve impulse (52)
cell morphogenesis involved in differentiation (47)
cell morphogenesis involved in neuron differentiation (43)
sensory perception of mechanical stimulus (29)
synaptic transmission (40)
cell projection organization (56)
cell projection morphogenesis (43)
neuron development (52)
inner ear development (27)
0 5 10 15 20
-Log10 (P-value)

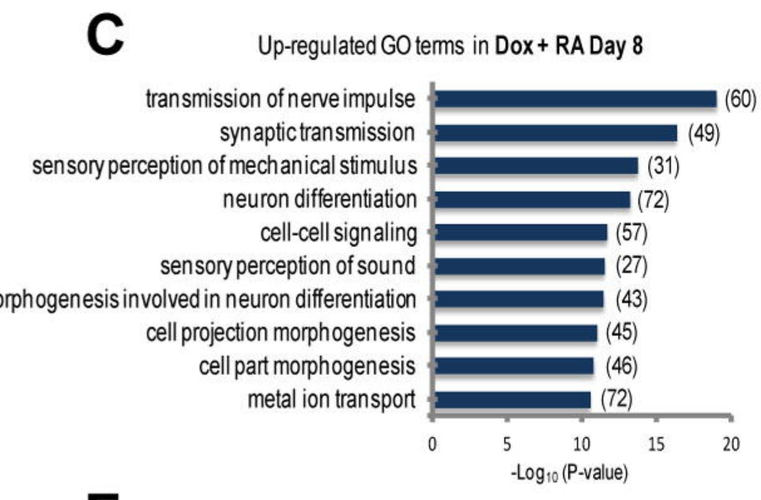
C
Up-regulated GO terms in Dox + RA Day 8
transmission of nerve impulse (60)
synaptic transmission (49)
sensory perception of mechanical stimulus (31)
neuron differentiation (72)
cell-cell signaling (57)
sensory perception of sound (27)
cell morphogenesis involved in neuron differentiation (43)
cell projection morphogenesis (45)
cell part morphogenesis (46)
metal ion transport (72)
0 5 10 15 20
-Log10 (P-value)

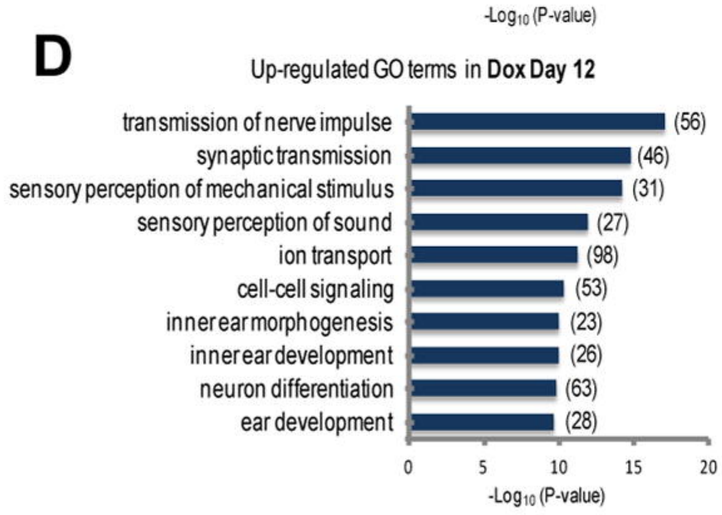
D
Up-regulated GO terms in Dox Day 12
transmission of nerve impulse (56)
synaptic transmission (46)
sensory perception of mechanical stimulus (31)
sensory perception of sound (27)
ion transport (98)
cell-cell signaling (53)
inner ear morphogenesis (23)
inner ear development (26)
neuron differentiation (63)
ear development (28)
0 5 10 15 20
-Log10 (P-value)

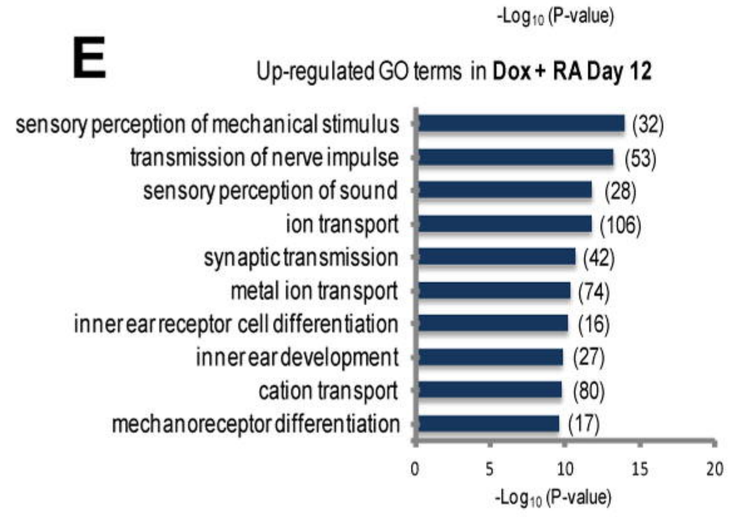
E
Up-regulated GO terms in Dox + RA Day 12
sensory perception of mechanical stimulus (32)
transmission of nerve impulse (53)
sensory perception of sound (28)
ion transport (106)
synaptic transmission (42)
metal ion transport (74)
inner ear receptor cell differentiation (16)
inner ear development (27)
cation transport (80)
mechanoreceptor differentiation (17)
0 5 10 15 20
-Log10 (P-value)

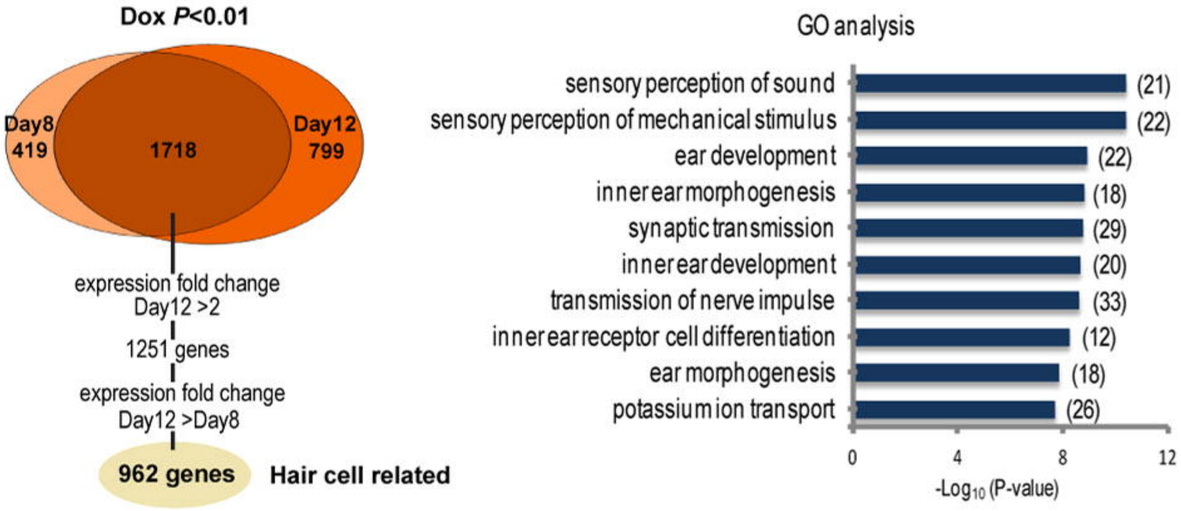
F
Up-regulated genes
Dox P<0.01
Day8
419
1718
Day12
799
expression fold change
Day12 >2
1251 genes
expression fold change
Day12 >Day8
962 genes
Hair cell related
GO analysis
sensory perception of sound (21)
sensory perception of mechanical stimulus (22)
ear development (22)
inner ear morphogenesis (18)
synaptic transmission (29)
inner ear development (20)
transmission of nerve impulse (33)
inner ear receptor cell differentiation (12)
ear morphogenesis (18)
potassium ion transport (26)
0 4 8 12
-Log10 (P-value)

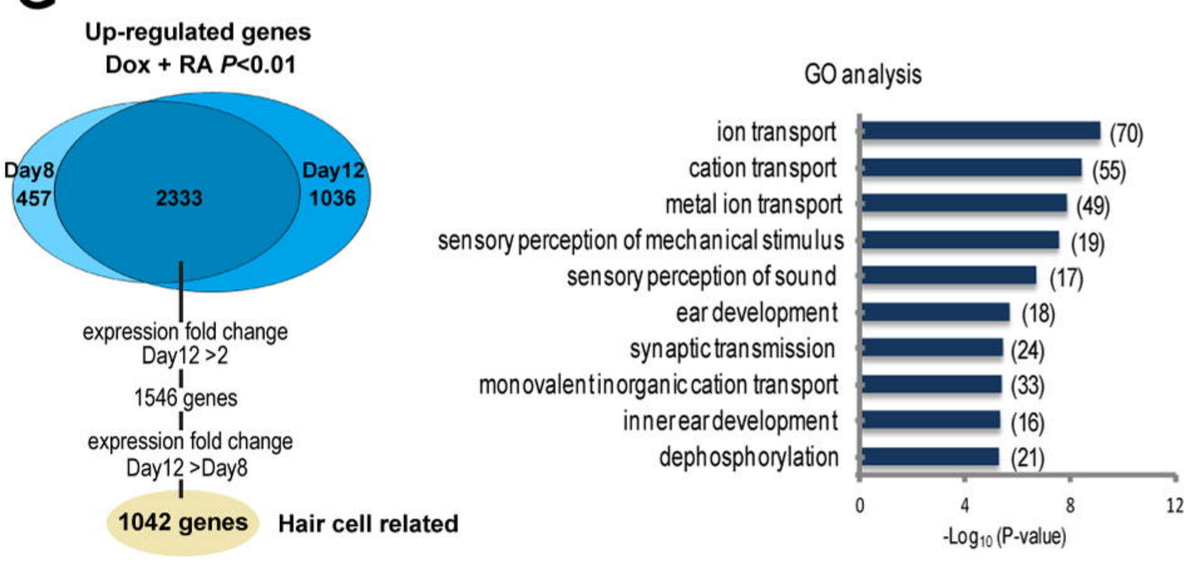
G
Up-regulated genes
Dox + RA P<0.01
Day8
457
2333
Day12
1036
expression fold change
Day12 >2
1546 genes
expression fold change
Day12 >Day8
1042 genes
Hair cell related
GO analysis
ion transport (70)
cation transport (55)
metal ion transport (49)
sensory perception of mechanical stimulus (19)
sensory perception of sound (17)
ear development (18)
synaptic transmission (24)
monovalent inorganic cation transport (33)
inner ear development (16)
dephosphorylation (21)
0 4 8 12
-Log10 (P-value)

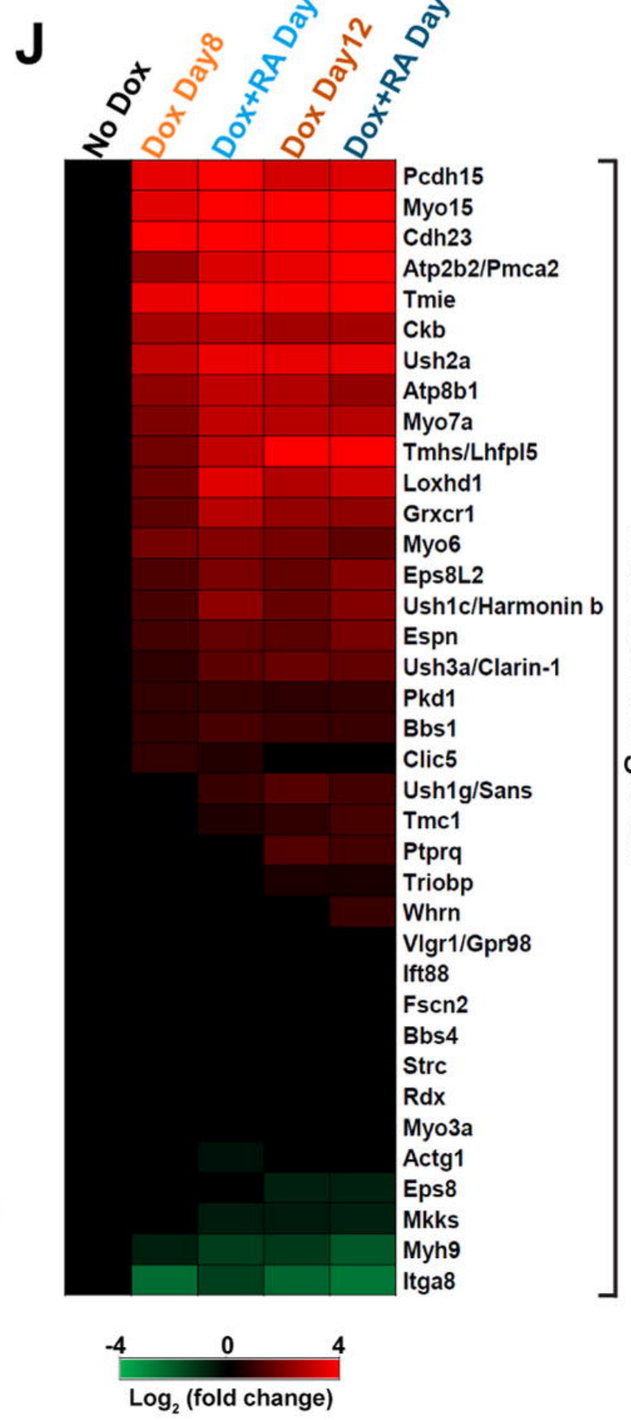
J
No Dox
Dox Day8
Dox+RA Day8
Dox Day12
Dox+RA Day12
Pcdh15
Myo15
Cdh23
Atp2b2/Pmca2
Tmie
Ckb
Ush2a
Atp8b1
Myo7a
Tmhs/Lhfpl5
Loxhd1
Grxcr1
Myo6
Eps8L2
Ush1c/Harmonin b
Espn
Ush3a/Clarin-1
Pkd1
Bbs1
Clic5
Ush1g/Sans
Tmc1
Ptprq
Triobp
Whrn
Vlgr1/Gpr98
Ift88
Fscn2
Bbs4
Strc
Rdx
Myo3a
Actg1
Eps8
Mkks
Myh9
Itga8
Hair bundle genes
-4 0 4
Log2 (fold change)

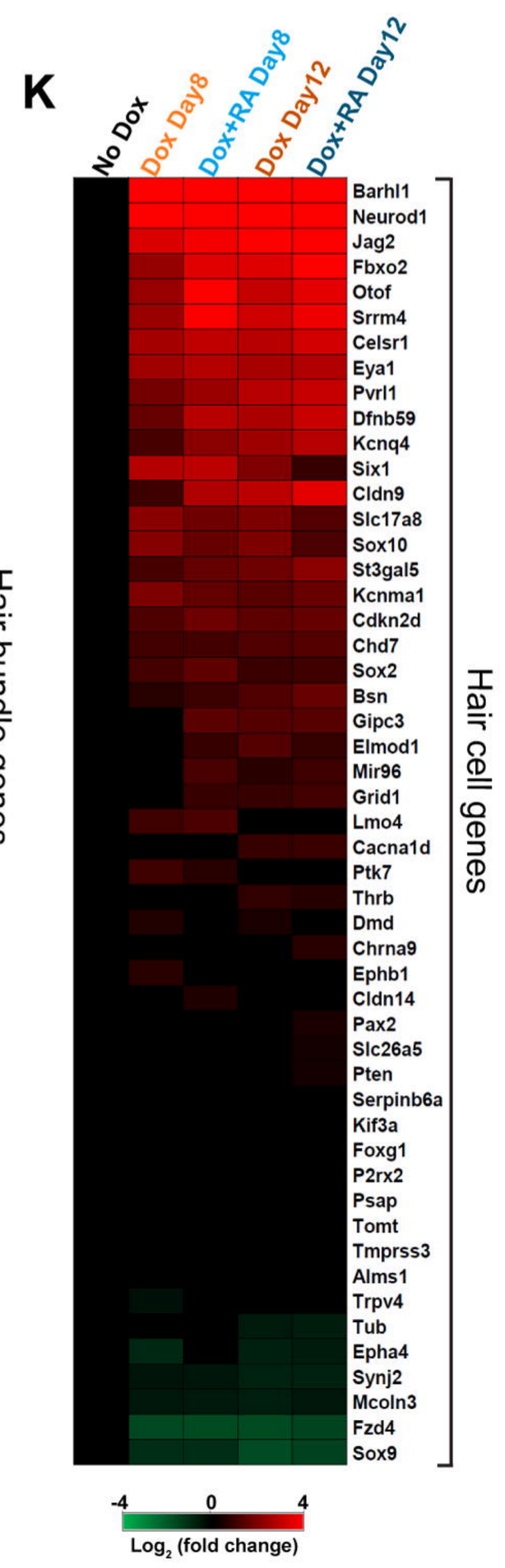
K
No Dox
Dox Day8
Dox+RA Day8
Dox Day12
Dox+RA Day12
Barhl1
Neurod1
Jag2
Fbxo2
Otof
Srrm4
Celsr1
Eya1
Pvrl1
Dfnb59
Kcnq4
Six1
Cldn9
Slc17a8
Sox10
St3gal5
Kcnma1
Cdkn2d
Chd7
Sox2
Bsn
Gipc3
Elmod1
Mir96
Grid1
Lmo4
Cacna1d
Ptk7
Thrb
Dmd
Chrna9
Ephb1
Cldn14
Pax2
Slc26a5
Pten
Serpinb6a
Kif3a
Foxg1
P2rx2
Psap
Tomt
Tmprss3
Alms1
Trpv4
Tub
Epha4
Synj2
Mcoln3
Fzd4
Sox9
Hair cell genes
-4 0 4
Log2 (fold change)

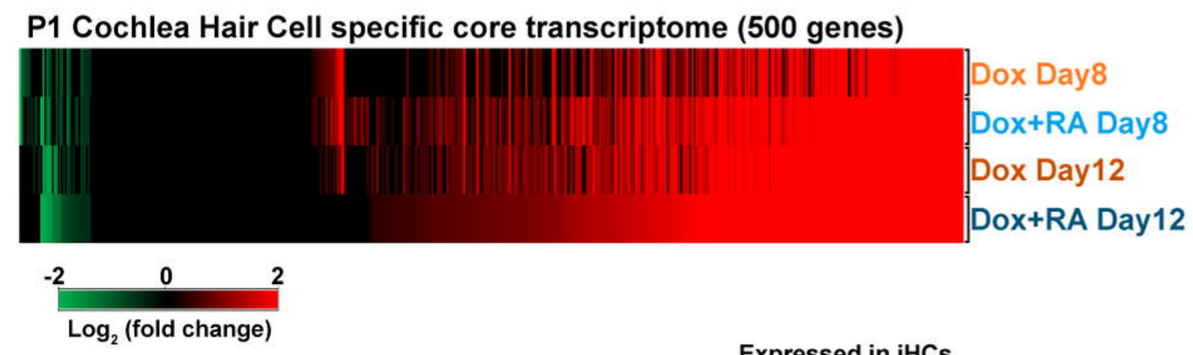
H
P1 Cochlea Hair Cell specific core transcriptome (500 genes)
Dox Day8
Dox+RA Day8
Dox Day12
Dox+RA Day12
-2 0 2
Log2 (fold change)

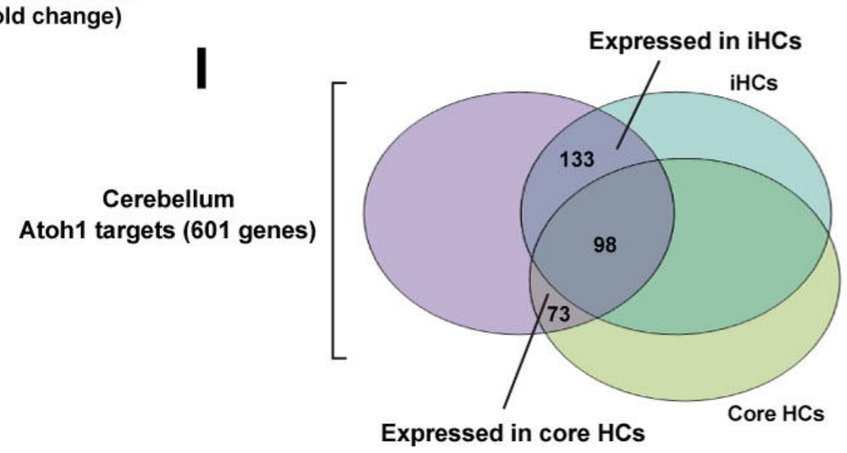
I
Cerebellum
Atoh1 targets (601 genes)
Expressed in iHCs
iHCs
133
98
73
Core HCs
Expressed in core HCs